ChemComm

REVIEW ARTICLE

View Article Online
View Journal | View Issue

Cite this: *Chem. Commun.*, 2026, **62**, 6696

Noncovalent interactions for enhancing organic electronic device function

Marina González-Sánchez, [a] Xinyi Wan, [a] Kyeong-Im Hong, [ab] Raúl González-Núñez [a] and Amparo Ruiz-Carretero *[a]

Received 26th January 2026,
Accepted 6th March 2026

DOI: 10.1039/d6cc00541a

rsc.li/chemcomm

Organic electronic device performance is increasingly recognized as an emergent property governed by molecular organization. This review highlights how noncovalent interactions enable precise control over molecular packing and nanoscale morphology in organic semiconductors. The key concept is the structure-function relationship, demonstrating that supramolecular chemistry is a crucial factor in achieving programmable, multifunctional and highly efficient devices. As design rules continue to mature and understanding of supramolecular order deepens, these strategies are poised to play a central role in the development of next-generation organic electronic devices with enhanced efficiency, stability, and functional richness.

Introduction

Electronic devices based on organic semiconductors (OSCs),[1–5] have experienced exponential scientific and technological growth since the invention of the organic light-emitting diode (OLED) in 1987.[6] These materials are composed of molecules featuring π-electrons delocalized along chains of conjugated double bonds or aromatic rings. This electronic delocalization not only confers structural stability but also significantly enhances their optical and electronic properties, such as light absorption and electrical conductivity, making π-functional systems key components in a wide range of technological applications.[7,8] In contrast to traditional inorganic semiconductors, organic devices offer unique competitive advantages, including mechanical flexibility, low weight, transparency and most notably, the ability to be processed from solution at low temperatures.[9–11] Representative technologies include OLEDs,[12–17] which currently dominate the display market for mobile devices; organic photovoltaic devices (OPVs),[18–25] which promise low-cost and sustainable solar energy conversion,

[a] *Instituto de Ciencia de Materiales de Madrid, Consejo Superior de Investigaciones Científicas CSIC, Sor Juana Inés de la Cruz 3, 28049, Madrid, Spain. E-mail: amparo.ruiz@csic.es*
[b] *Instituto Madrileño de Estudios Avanzados en Nanociencia (IMDEA Nanociencia), Calle Faraday 9, 28049, Madrid, Spain*

Marina González-Sánchez

Marina González-Sánchez obtained her PhD in Organic Chemistry in 2025 from the Universidad Autónoma de Madrid (UAM), under the supervision of Prof. David González Rodríguez. Her doctoral research focused on the study of self-assembled architectures based on nucleobase pairing. She is currently a postdoctoral researcher at the Institute of Materials Science of Madrid (ICMM-CSIC), working in the group of Dr. Amparo Ruiz-Carretero, where her research centers on supramolecular chemistry, organic semiconductors, and functional self-assembled materials for electronic and optoelectronic applications.

Xinyi Wan

Xinyi Wan obtained her master's degree in Chemistry in 2022 from Northeastern University (China). Her research was focused on chiral liquid crystals to study the effects of different core structures and terminal substituents on liquid crystalline behavior. She is currently a PhD student under the supervision of Dr. Amparo Ruiz-Carretero and Dr. Berta Gómez-Lor Pérez at the Institute of Materials Science of Madrid (ICMM-CSIC), with a particular focus on supramolecular chemistry, the chiral-induced spin selectivity (CISS) effect and the development of organic semiconductor materials.

organic field-effect transistors (OFETs),[26–30] which are essential for the development of flexible electronic circuits[17–20] and organic thermoelectric devices.[31] Furthermore, the versatility of organic synthesis enables the design of materials, allowing fine tuning of parameters such as the energy gap, frontier orbital levels (HOMO and LUMO) and solubility through precise molecular modifications.[32–34] Nevertheless, one of the main challenges in organic electronics lies in the fact that charge-transport properties and device efficiency do not depend solely on the individual molecular structure,[35,36] but rather on how these molecules organize in the solid state.[37] Device performance is often limited by low charge-carrier mobility and the instability of active layers, issues that primarily originate from structural disorder and morphological defects in thin films. Such defects act as charge traps, hindering electron/charge transport and negatively impacting key photophysical processes, including exciton diffusion.[38–44] In this context, controlling molecular packing and nanoscale organization becomes an essential requirement to optimize both charge injection and transport.[32,45–47] The generation of well-defined donor(D)–acceptor(A) interfaces with nanometric precision is particularly critical to maximize exciton dissociation before recombination.[48–50] Likewise, the creation of ordered and well-connected transport pathways constitutes a fundamental pillar for improving power conversion efficiency in OPVs and switching frequency in OFETs.[32,37,51–56] In this sense, the integration of noncovalent interactions into the design of electronic materials has given rise to the field of supramolecular electronics,[57] which aims to bridge the gap between the electronics of individual molecules and that of macroscopic thin films.[37,58,59] In organic materials, these supramolecular interactions, primarily van der Waals forces,[60] π–π stacking[37,61–63] and hydrogen bonding (H-bonding),[64–67] are intrinsically weaker than covalent bonds, yet they play a crucial role in the formation of functional nanostructures.[68,69] Although their binding energies are significantly lower than those of covalent bonds, their reversible and cooperative nature endows materials with dynamic behavior,[70,71] enabling structural error correction, responsiveness to external stimuli and, in some cases, self-healing properties.[72] Through the strategic use of interactions such as H-bonding, aromatic stacking, solvophobic forces or metal coordination, it is possible to program the self-assembly of π-conjugated molecules into well-defined hierarchical architectures, including one-dimensional nanowires,[73,74] nanotubes[75,76] or two-dimensional crystalline networks.[77–79]

These architectures optimize π-orbital overlap and facilitate charge transport, thereby overcoming the limitations inherent

Kyeong-Im Hong

Kyeong-Im Hong got her PhD degree in Chemistry (2020) under supervision of Prof. Woo-Dong Jang at Yonsei University (South Korea). Her research was focused on supramolecular chemistry based functional materials to develop artificial molecular receptors, supramolecular catalysis, and stimuli-responsive materials. She is currently a postdoctoral researcher under supervision of Dr. Amparo Ruiz-Carretero at ICMM-CSIC combined with co-supervision of Prof. Thomas M. Hermans at IMDEA Nanociencia to investigate the efficiency of organic photovoltaic materials through understanding the relationship between supramolecular chiral materials and spin selectivity (CISS effect).

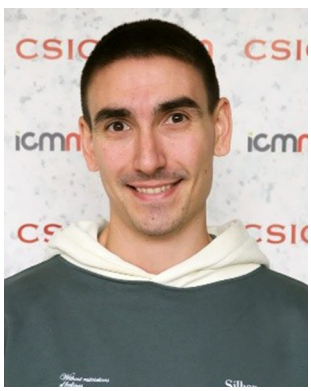

Raúl González-Núñez

Raúl González-Núñez obtained his PhD in Materials and Nanotechnology in 2025 from the University of Málaga (UMA), under the supervision of Prof. Rocío Ponce Ortiz and Prof. M. Carmen Ruiz Delgado. His research aimed to explore critical questions about how charge transport properties are influenced by structural modifications and supramolecular interactions that govern the performance of electronic devices. He is currently a postdoctoral researcher at the Institute of Materials Science of Madrid (ICMM-CSIC) under the supervision of Dr. Amparo Ruiz-Carretero, where his research focuses on the development of next-generation organic photovoltaic materials.

Amparo Ruiz-Carretero

Amparo Ruiz-Carretero is an ATRAE Senior Researcher at the Institute of Materials Science of Madrid at the Spanish Research Council (ICMM-CSIC). She studied chemistry and obtained her PhD at the University of Castilla–La Mancha, after several internships in the groups of Profs. E. W. Meijer and A. Schenning. After postdoctoral work with Prof. S. Stupp at Northwestern University and Prof. L. De Cola at the University of Strasbourg, she obtained a CNRS position in 2015 at Institute Charles Sadron. Her independent research focuses on supramolecular chemistry for organic electronics. In 2024, she secured an ATRAE project to join CSIC, where her group studies supramolecular chirality and spin selectivity for energy technologies.

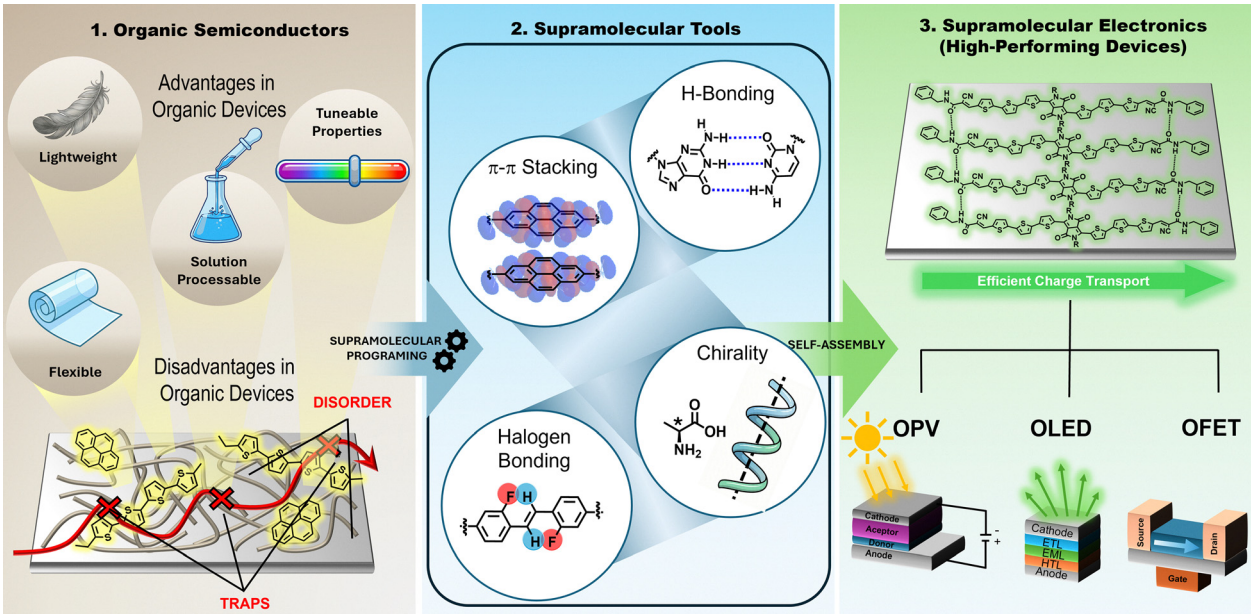

Fig. 1 Schematic representation of the role of supramolecular chemistry in the transition from conventional organic semiconductors (OSCs) to high-performance electronic devices. (1) OSCs offer advantages such as low weight, mechanical flexibility, solution processability and tuneable properties; however, they often suffer from structural disorder, which generates charge traps that limit charge transport and device performance. (2) Supramolecular tools such as π–π stacking, H-bonding, chirality and halogen bonding enable controlled molecular self-assembly. (3) The resulting supramolecular organization leads to highly ordered architectures that facilitate efficient charge transport and translate into high-performance devices, including OPVs, OLEDs, and OFETs.

to amorphous or highly disordered systems (Fig. 1). The formation of such architectures is governed by thermodynamically controlled self-assembly processes,[80–83] in which the information encoded within the building blocks determines the final structure.[84,85] This further enables the generation of hierarchical superstructures that are sensitive to external stimuli such as pH, temperature or light, providing the materials with emergent properties that are absent in their individual components.[58,70] In this review, we provide a perspective on how noncovalent interactions can be deliberately harnessed as design elements to control molecular organization and device performance in organic electronics. We first discuss π–π stacking as the fundamental structural motif governing charge transport in organic semiconductors, highlighting representative systems where controlled stacking leads to high mobility and efficient optoelectronic response. We then examine H-bonding as a versatile and programmable interaction that enables hierarchical self-assembly, morphology stabilization, and enhanced charge separation in devices. Subsequent sections address fluorination strategies and supramolecular chirality, emphasizing how subtle noncovalent effects can modulate electronic structure, spin-selective transport, and emergent functionalities. Finally, we briefly survey additional noncovalent interactions beyond π–π stacking and H-bonding, and conclude with an outlook on future challenges and opportunities toward predictive supramolecular design of next-generation organic electronic devices.

More importantly, we show that noncovalent interactions are not merely low-cost processing strategies, but precision engineering tools that enable deep control over molecular architecture and conjugation pathways, paving the way toward programmable, multifunctional and highly efficient organic electronic devices.[9,86,87]

Noncovalent interactions as design tools in organic electronics

π–π Stacking in organic electronic devices

Aromatic π–π stacking interactions are intrinsic to essentially all OSCs and therefore constitute a common structural motif throughout the materials discussed in this and the following sections. Accordingly, when alternative noncovalent interactions are highlighted, π–π stacking should be understood as being inherently present unless explicitly stated otherwise. Nevertheless, given its central role in dictating molecular organization and charge-transport behaviour, we devote this section specifically to π–π stacking in order to highlight representative studies that have shaped current design strategies in organic electronic devices. Aromatic π–π stacking interactions constitute a fundamental driving force in the organization of semiconducting supramolecular systems, as they enable the formation of architectures with outstanding charge-transport and optical response properties.[88,89] Unlike covalent polymers, these systems rely on the efficient overlap of the π-electron clouds of planar aromatic cores, which promotes the delocalization of charge carriers and excitons along self-assembled columns.[1,90] An example of this strategy is provided by

nanographenes and large polycyclic aromatic hydrocarbons, such as hexa-peri-hexabenzocoronene (HBC), whose highly symmetric structure favours the formation of well-defined discotic columnar assemblies.[91–93] Such organization is crucial for optimizing charge transport in FETs and improving efficiency in OPVs.[94] In this context, the rational design of the aromatic core, through control of its size, symmetry and topology, enables precise modulation of the HOMO–LUMO gap and directs molecular orientation on the substrate, either in edge-on or face-on configurations, to maximize electronic coupling along the desired functional direction. Research carried out by Müllen and co-workers[94–96] has established nanographenes, particularly HBC derivatives (Fig. 2a), as benchmark materials in organic electronics due to their strong tendency to self-assemble into highly ordered columnar nanostructures through π–π stacking interactions. With regard to charge transport, exceptional local mobility values exceeding 1.1 $cm^2\ V^{-1}\ s^{-1}$ were found in the crystalline phase of HBC-C_{14}, significantly outperforming previously reported discotic systems.[96] At the device level, OFETs fabricated with aligned layers of similar HBCs exhibited hole mobilities on the order of 5×10^{-3} $cm^2\ V^{-1}\ s^{-1}$ with on/off ratios approaching 10^4 and their incorporation in OPV devices enabled external quantum efficiencies of up to 34%, highlighting the relevance of controlled π–π stacking for optoelectronic performance. Along these lines, further advances have demonstrated that π–π stacking can be exploited not only to form columnar assemblies, but also to engineer more complex bicontinuous (D/A) architectures through molecular design. In this context, research by Aida and co-workers,[76,97–100] showed that amphiphilic molecular design constitutes an effective strategy to achieve such organization *via* precise control of π–π stacking, while suppressing the formation of charge-transfer (CT) complexes that act as carrier traps. A key milestone of this approach was the development of coaxial nanotubes of HBC-trinitrofluorenone (TNF) dyads, in which a densely packed HBC donor wall is coated by an acceptor TNF layer (Fig. 2b).[76] These nanostructures exhibited a rapid photoconductive response, with on/off ratios exceeding 10^4 and intratubular charge mobilities of up to 3 $cm^2\ V^{-1}\ s^{-1}$.[100] Complementarily, the use of amphiphilic/lipophilic oligothiophene-C_{60} dyads enabled the spontaneous formation of lamellar liquid-crystalline phases that provided long-range conductive pathways and effectively suppress trap sites (Fig. 2d). As a result, these systems achieved photoconductivity values an order of magnitude higher than those of non-amphiphilic analogues.[97] Research by Wasielewski and co-workers[101–107] has focused on the design of highly ordered supramolecular architectures to optimize charge generation, separation, and transport in photovoltaic systems. A central element of this strategy is the use of perylenediimide (PDI) derivatives as acceptors, whose strong propensity for π–π stacking promotes the formation of segregated electronic channels. Structural studies using X-ray scattering techniques demonstrated that supramolecular order is a decisive factor governing electronic behaviour: in PDI-DPP-PDI thin films (Fig. 2c, top), solvent vapor annealing induces a transition to a highly crystalline phase that extends the lifetime of free charge carriers to the millisecond regime, in contrast to the ultrafast recombination observed in disordered phases.[102] In related systems, such as ZnP-PDI dyads and more complex

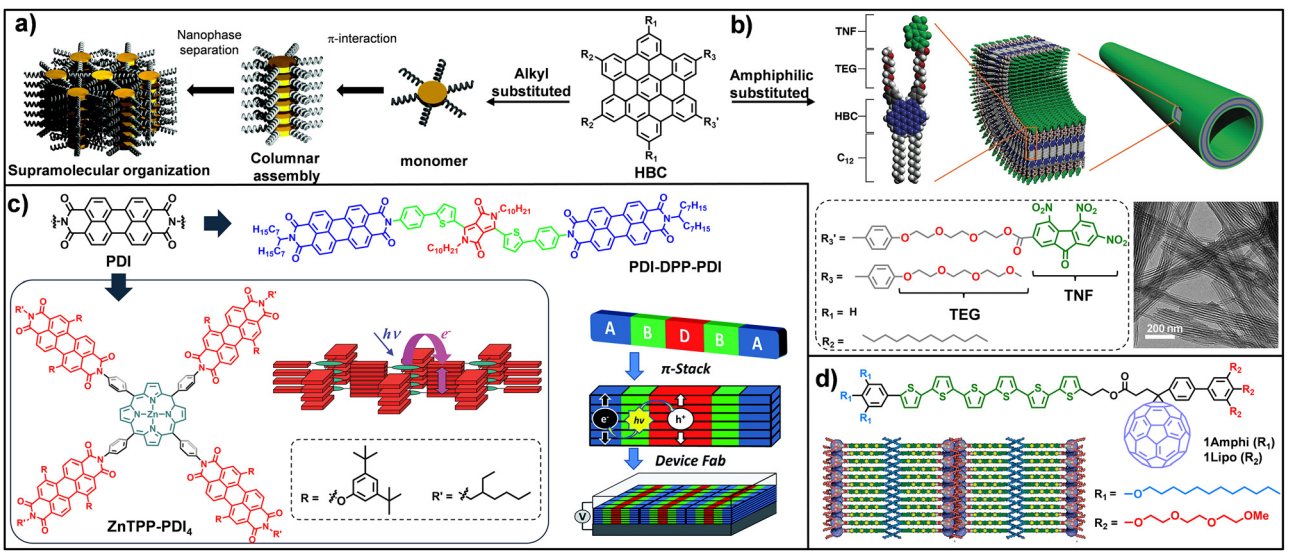

Fig. 2 (a) Schematic illustration of the supramolecular organization processes of alkyl-substituted HBC. (b) Schematic representations of molecular structure and self-assembly of HBC-TNF system and TEM image of nanotubes. (c) Molecular structure of PDI-DPP-PDI (top) and schematic depiction of the self-assembly of a covalent donor–bridge–acceptor (D–B–A) system designed to control charge separation and generate spatially segregated electron and hole-transport pathways. Molecular structure of ZnTPP–PDI_4 (bottom) and schematic representation of the self-assembled architecture. (d) Molecular structures of 1Amphi and 1Lipo with schematic representations of their preferred molecular orientations in the assembled state. Adapted from ref. 96, 76, 102, 105 and 97 with permission from Copyright 2007-American Chemical Society, 2006-AAAS, 2015-Royal Society of Chemistry, 2002 and 2008-American Chemical Society respectively.

architectures (ZnTPP-PDI_4), ordered self-assembly enables high free-carrier yields and ultrafast electron transfer rates (up to 2.4×10^{10} s^{-1}),[103] demonstrating that charge delocalization along π–π stacked columns is key to overcoming the initial Coulombic attraction (Fig. 2c, bottom).[105] Taken together, these studies establish forced π–π stacking as an essential structural principle for achieving efficient charge separation and long-range electronic transport. Collectively, these studies demonstrate that enforced and directional π–π stacking is the primary structural determinant of efficient charge delocalization and long-range transport in organic semiconductors, transforming molecular design into macroscopic device performance.

Role of hydrogen bonds in organic electronic devices

Within the broad family of noncovalent interactions, H-bonding is one of the most effective interactions for supramolecular control, as it enables reversible, highly directional associations with nanometric precision.[108,109] Although individually a weak interaction, its tunability and specificity make it a key element for enforcing molecular conformation, planarity and predictable solid-state packing-features that are difficult to achieve using dispersion forces or isolated π–π stacking alone.[64,110–114] In the context of OSCs, H-bonding has thus evolved from a purely structural motif into a central strategy for directing the self-assembly of D/A architectures, simultaneously optimizing morphology, nanometric connectivity, and charge-transport pathways.[115–117] Early studies established H-bonding as a means of enforcing one-dimensional order and cooperative self-assembly in π-conjugated systems. Initial illustrative examples arise from the work of Stupp and co-workers,[118,119] who demonstrated that hairpin-shaped molecules functionalized with H-bonding motifs, based on sexithiophene units and a *trans*-1,2-diamidocyclohexane (DACH) core, self-assemble into grooved nanowires with a uniform diameter of approximately 3.0 nm. FT-IR and variable-temperature NMR studies confirmed that H-bonds cooperate with π–π stacking to restrict molecular rotation and promote long-range hierarchical order. This packing arrangement enables the coexistence of H- and J-type aggregates, broadening the optical absorption window and enhancing light harvesting. OFET measurements revealed that thin films of molecule M1 processed from solvents that favour H-bond-driven self-assembly exhibit a hole mobility of 3.46×10^{-6} cm^2 V^{-1} s^{-1}, representing an order-of-magnitude enhancement compared to devices in which this supramolecular organization is not induced.[118] In OPV devices, the hairpin architecture allows fullerenes to be accommodated within the grooves of the nanowires in a receptor-ligand-like configuration, optimizing the heterojunction interface and yielding a power conversion efficiency (PCE) outperforming the analogue lacking H-bonding motifs.[119] These foundational examples paved the way for more systematic investigations into how H-bonding can be used to engineer morphology and electronic connectivity. Other studies have been particularly influential in consolidating this interaction as a tool for morphological and electronic control in organic optoelectronic devices.[120,121] This research work is coherently built around derivatives of diketopyrrolopyrrole (DPP), a benchmark chromophore in the field. Within this framework, a variety of supramolecular strategies have been introduced to elucidate how H-bonding governs hierarchical organization, nanometric connectivity and charge transport.[122] A foundational result is the design of the hairpin-shaped molecule DPPHP (Fig. 3a),[120] which incorporates a DACH core as a self-assembly motif and two conjugated DPP arms. The synergistic interplay between H-bonding and π–π stacking enables the formation of long and robust supramolecular nanowires (100–700 nm), which act as efficient charge transport pathways. This system demonstrated that device performance depends critically on the thermodynamic assembly pathway, requiring a stepwise strategy in which the D molecule is preorganized prior to A addition. AFM and cryo-TEM confirmed the preservation of the supramolecular network, resulting in a 45% increase in hole mobility and efficiency enhancements exceeding 50% relative to H-bond-free controls. Comparative molecular design provided direct evidence that these effects originate from H-bonding rather than crystallinity alone. Subsequent comparative studies, in which an amide was replaced by an ester at equivalent positions of the DPP scaffold, allowed the supramolecular contribution of H-bonding to be isolated (Fig. 3b). While ester derivatives exhibited excessive crystallinity and large domains, H-bonding in the amide analogues effectively competed with extensive π–π stacking, promoting short, interconnected fibres and a more homogeneous nanoscale morphology. These differences translated into a doubling of hole mobility and PCE improvement of up to 50% (4.9% *vs.* 2.8%).[121] Beyond morphology control in OPVs, H-bonding has also proven highly effective in tuning charge transport in field-effect devices. Later studies extended the role of H-bonding to other optoelectronic devices. Its versatility was demonstrated in OFETs based on DPP derivatives functionalized with triazatruxene units (Fig. 3c),[123] where the *in situ* formation of highly robust N–H···O=C networks in the solid state led to compact crystalline packing (π–π ≈ 0.30 nm) and two-orders-of-magnitude increases in hole mobility. More recently, reports of our group revealed that H-bonding not only controls morphology but also dramatically extends charge-carrier lifetimes and modulates the intrinsic electronic nature of the semiconductor. The topology of the amide groups (C- or N-centered) dictates the formation of J-type aggregates (Fig. 3d), highly interconnected fibrillar networks, and photoconductivity an order of magnitude higher, with carrier lifetimes at least ten times longer and OFET mobilities on the order of 10^{-2} cm^2 V^{-1} s^{-1} compared to inactive controls.[124] Furthermore, direct participation of the DPP lactam carbonyl in H-bonding favours linear over cross conjugation, facilitating solid-state redox processes and the generation of stable charged species.[87] Importantly, these studies reveal that not only the presence but also the strength and dynamics of H-bonding are decisive. Finally, replacing amides with ureas confirmed that not only the presence but also the position and dynamic nature of the supramolecular motif are decisive.[125] Ureas anchored to the DPP core promote more efficient electronic connectivity,

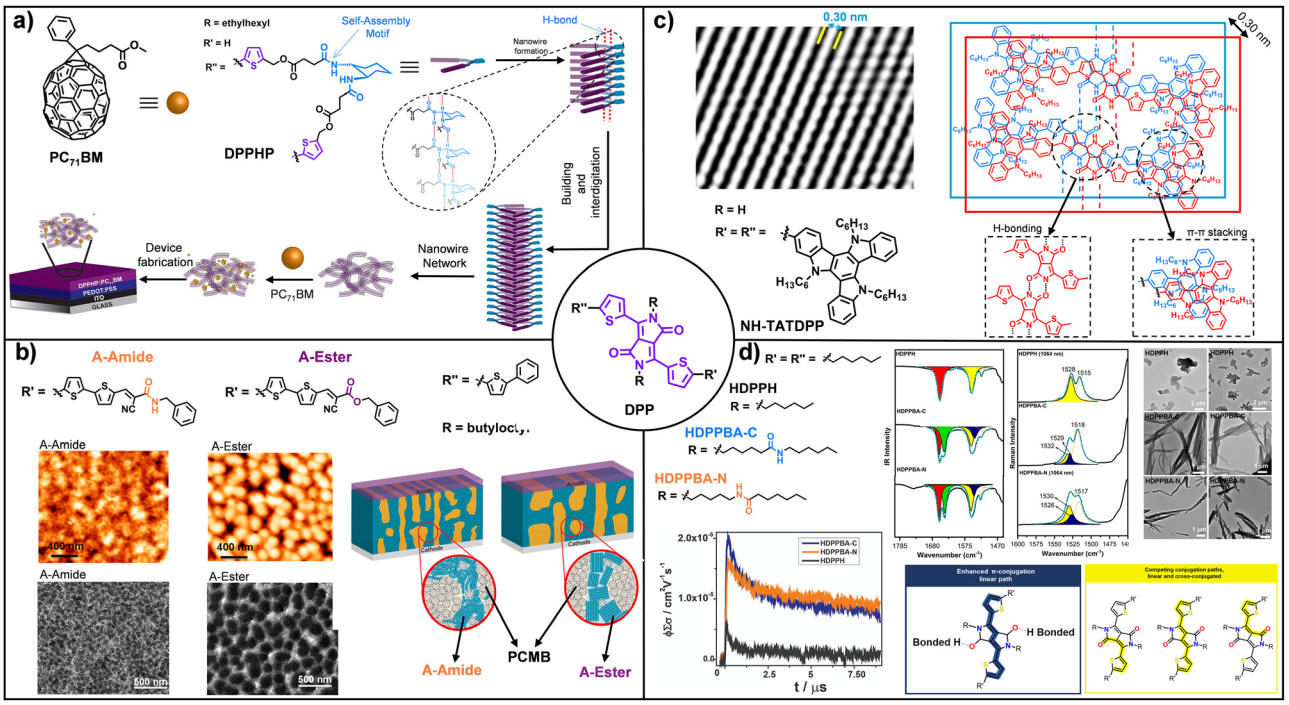

Fig. 3 (a) Molecular structure of the hairpin-shaped DPP derivative (DPPHP), highlighting the self-assembly motif (blue) and molecular structure of $PC_{71}BM$. Schematic illustration of the preparation pathways employed for device fabrication. (b) Molecular structures of A-amide and A-ester and AFM images of donor:$PC_{71}BM$ and TEM images and schematic representation of the active-layer morphology in devices based on A-amide and A-ester. (c) Molecular structure of NH-TATDPP and schematic representation of its proposed supramolecular arrangement. Processed HR-TEM image from the square part. (d) Molecular structures of HCPPH, HDPPBA-C and HDPPBA-N and FTIR spectra (left) and Raman spectra (right) recorded as solid powders and TEM images. Schematic representation of π-conjugation pathways showing (left) competing linear and cross-conjugated routes in the absence of H-bonding and the enhanced linear π-conjugation enabled by H-bond formation through the lactam carbonyl group (right). Kinetic traces of photoconductivity transients. Adapted from ref. 120, 123, 121, 87 and 124 with permission from Copyright 2013-Royal Society of Chemistry, 2019-Chemistry Europe, 2015-American Chemical Society, 2024-Royal Society of Chemistry and 2023-American Chemical Society, respectively.

whereas excessively rigid H-bond networks can hinder charge transport, as evidenced by enhanced photoconductivity upon partial weakening of the H-bonds. Another relevant study incorporating urea motifs into DPP-based polymers was reported by Liu and Zhang, who demonstrated that side-chain engineering through the introduction of urea groups constitutes a highly effective strategy for enhancing the semiconducting performance of DPP4T conjugated polymers.[126] In this work, a series of polymers was synthesized in which the fraction of urea-bearing side chains was systematically varied, confirming the formation of intermolecular H-bonding networks. In OFET devices, the polymer pDPP4T-3 exhibited a hole mobility of 13.1 $cm^2\ V^{-1}\ s^{-1}$, a value that remains remarkable even by current standards and highlights the strong potential of supramolecular side-chain engineering. In OPV applications, these materials also delivered substantial performance improvements as D derivatives in blends with $PC_{71}BM$ (A), with the pDPP4T-1 system achieving PCE of 6.8%, significantly outperforming reference polymers lacking urea functionalities. Structural characterization by Grazing Incidence X-Ray Diffraction (GIXRD) and Scanning Transmission Electron Microscopy (STEM) revealed that H-bonding not only reinforces lamellar ordering of the alkyl side chains, but also promotes more defined π–π interactions and the formation of interconnected nanofibers up to 50 nm in width. Importantly, many of these studies highlight that H-bonding and π–π stacking rarely operate in isolation. Instead, efficient supramolecular semiconductors often arise from their concerted action, where directional H-bonding programs the relative positioning and connectivity of the molecular building blocks, while π–π stacking ensures strong electronic coupling and charge delocalization. A complementary example is provided by Frauenrath *et al.*,[127] who demonstrated that directional H-bonding in perylene bisimides (PBI) functionalized with oligopeptide side chains enables precise control over the self-assembly of organic nanowires (Fig. 4a). FT-IR spectroscopy confirmed that L-alanine units induce parallel β-sheet-type aggregation, which cooperates with π–π stacking of the aromatic core to generate well-defined one-dimensional architectures. A key finding was the observation of a "double" odd-even effect in circular dichroism (CD) spectra, whereby both the intensity and sign of supramolecular chirality depend on the number of L-alanine units and the length of the alkyl spacer. This supramolecular organization had a direct impact on CT in OFETs based on derivatives with an odd number of alanines exhibited more constructive π-overlap and achieved electron mobilities an order of magnitude higher than their even analogues. This study highlights that the mere formation of 1D aggregates is

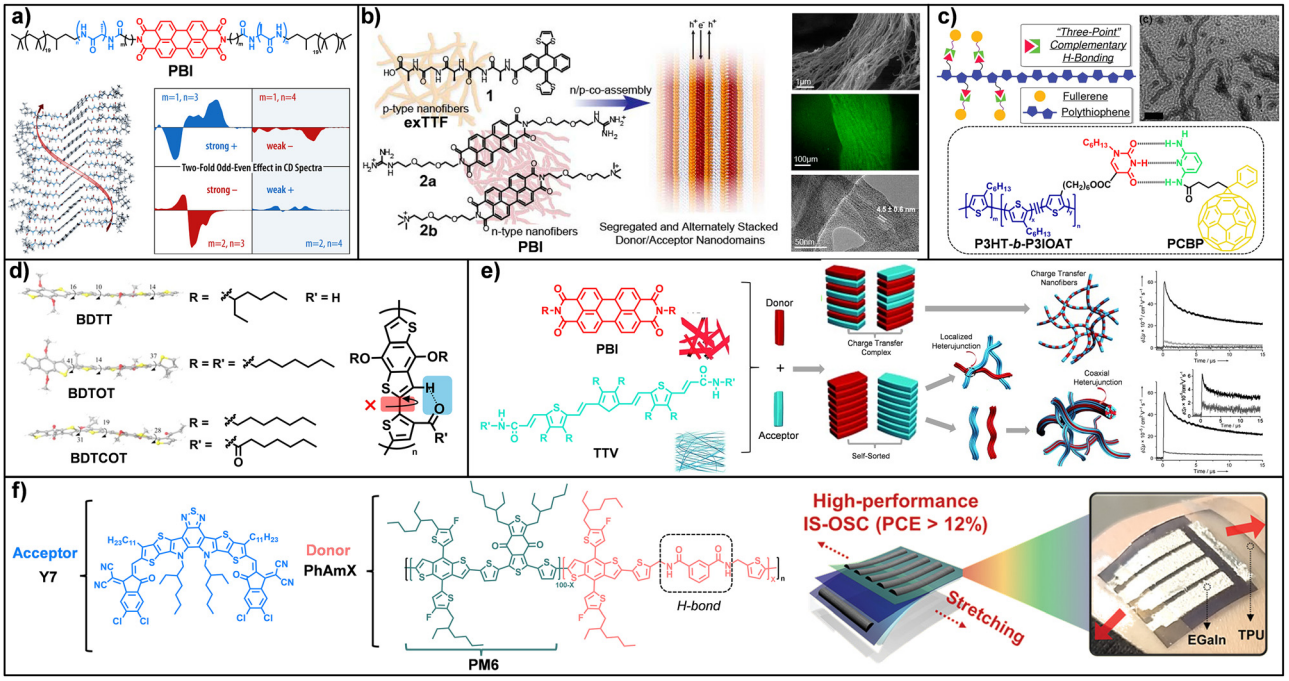

Fig. 4 (a) Molecular structures of **PBI** derivatives and MD simulations illustrating stable supramolecular arrangement. CD spectra reveal pronounced odd-even in the Cotton effect sign. (b) Molecular structures and schematic nanoarchitectures of **exTTF** derivative and **PBI** derivatives. Schematic representation of the n/p-type material obtained *via* co-assembly of the preorganized components. SEM images, confocal fluorescence micrograph and TEM of the co-assembled membrane. (c) Molecular structures and schematic representation of H-bonding between **P3HT-*b*-P3IOAT** and **PCBP** and TEM images. (d) Molecular structures of BDTT and its derivatives, together with their minimum-energy conformations. (e) Molecular structures of **PBI** and **TTV**, and a conceptual scheme illustrating possible hierarchical assemblies arising from interactions between p-type donors and n-type acceptors. FP-TRMC photoconductivity (top) transients of **TTV** (light gray), **PBI** (dark gray) and **TTV/PBI** (1:1; black) films. FP-TRMC photoconductivity (bottom) spectra of a **TTV/PBI** (1:1) film prepared from *n*-decane. (f) Molecular structures of **Y7** molecule acceptor and **PM6**, **PhAmX** polymer donors and overview of intrinsically stretchable organic solar cells (IS-OSCs). Adapted from ref. 127, 128, 129, 131, 132, 137 and 139 with permission from Copyright 2014, 2013-American Chemical Society, 2015-Elsevier, 2015, 2014 and 2022 Wiley-VCH GmbH, respectively.

insufficient; rather, H-bonding dictates the fine geometry of electronic overlap required for efficient charge transport. Another major advance in the use of H-bonding as a supramolecular organizing tool is the ionic co-assembly system of n/p nanofibers developed by the group of N. Martín.[128] This work represents the first example of highly ordered functional n/p materials obtained *via* electrostatic co-assembly of preformed complementary nanofibers. In this hierarchical system, H-bonding initially directs the individual formation of p- and n-type nanofibers, while oppositely charged surfaces subsequently induce periodic alignment at the mesoscale. Organization occurs through two well-defined stages: a cooperative H-bond network, reinforced by π–π stacking between **exTTF** units, yields rigid and uniform p-type nanofibers bearing negatively charged carboxylate groups, while the n-type component consists of PBI derivatives functionalized with ammonium or guanidinium groups, imparting positive charge. Mixing both systems triggers immediate ionic self-assembly into highly ordered architectures. Electron microscopy and X-ray scattering confirmed the formation of segregated and alternating D/A nanodomains with a well-defined periodicity of approximately 4–5 nm, an optimal length scale for minimizing charge recombination. As a direct consequence of this high level of supramolecular order, charge mobility values of up to 0.8 $cm^2 V^{-1} s^{-1}$ were achieved. A complementary strategy to simultaneously control morphology and thermal stability in organic solar cells was developed by Qin and co-workers,[129–131] who introduced a supramolecular recognition system based on complementary three-point H-bonding. In this approach, polythiophene block copolymers functionalized with isoorotic acid (IOA) are combined with fullerene derivatives bearing diaminopyridine units, enabling specific anchoring of the A molecule along the D chains. This molecular programming directs the formation of core-shell nanofibers, in which the crystalline P3HT core is surrounded by IOA-and fullerene-rich domains, as confirmed by microscopy and Nuclear Magnetic Resonance (NMR). Grazing Incidence Small and Wide Angle X-Ray Scattering (GISAXS and GIWAXS) further revealed long-range nanometric order (32–41 nm) absent in conventional bulk heterojunctions (BHJs) (Fig. 4c). This cooperation between polymer crystallization, block-copolymer phase separation, and H-bond-mediated fullerene aggregation yielded devices with efficiencies of up to 2.87% in ternary blends and, notably, markedly enhanced thermal stability. Unlike standard P3HT/PCBM systems, these devices retained more than 60% of their initial efficiency after 112 h at 110 °C, demonstrating that H-bonding can act as an effective morphological stabilizer against thermal degradation. Kim, Woo, and co-workers[132] investigated how side-chain

engineering in benzodithiophene-thiophene (BDT-T) copolymers can dramatically improve OPV performance through the incorporation of intramolecular H-bonding (Fig. 4d). They designed the polymer BDTCOT, which exhibits a conformational locking interaction between the carbonyl oxygen and a neighbouring BDT-hydrogen. Density functional theory (DFT) calculations showed that this interaction reduces backbone torsion, significantly enhancing planarity and promoting more efficient intermolecular organization compared to analogues bearing conventional alkyl side chains. GIWAXS measurements revealed that BDTCOT exhibits the shortest π–π stacking distance in the series (3.72 Å in blend films), facilitating more efficient charge transport. In organic solar cells, BDTCOT:$PC_{71}BM$ devices achieved a PCE of 4.66%, substantially outperforming the 2.52% and 2.68% PCEs obtained for BDTT and BDTOT, respectively. This improvement was attributed to the combined enhancement of the open-circuit voltage (V_{oc}) and the short-circuit current (J_{sc}) arising from the improved morphology and planarity induced by H-bonding. In multicomponent systems, H-bonding further enables self-sorting strategies, promoting selective recognition between complementary components and preventing disordered mixing.[133–135] This principle is particularly relevant in BHJs, where controlled D/A segregation is crucial to minimize charge recombination and ensure continuous transport pathways.[136] A representative example is the work of Ajayaghosh *et al.*,[137] who exploited directional H-bonding to induce self-ordering in organic devices (Fig. 4e). In this system, an amide-functionalized trithienylenevinylene (TTV) unit acts as a p-type semiconductor with a strong propensity for one-dimensional H-bond-mediated self-assembly, while the n-type component, a PBI, predominantly assembles *via* π–π stacking. The coexistence of these assembly modes leads to molecular self-sorting that suppresses the formation of CT complexes, which often quench photocurrent, and instead promotes hierarchical mesoscale organization. The system evolves into aligned coaxial fibres with well-defined p–n heterojunctions, preserving independent charge-transport channels. UV/Vis spectra and XRD patterns confirmed that each component retains its characteristic packing modes, ruling out CT complex formation. As a direct consequence of this supramolecular organization, Flash Photolysis Time-Resolved Microwave Conductivity (FP-TRMC) measurements revealed up to a twelvefold increase in photoconductivity for the bicomponent **TTV/PBI** system relative to the isolated donor. The work by Lee, Kim, and co-workers represents a significant advance in the development of intrinsically OSCs, demonstrating that large mechanical deformations can be accommodated without loss of functionality, while maintaining high photovoltaic performance through the rational use of H-bonding.[138] In this study, a family of D polymers, termed **PhAmX**, was designed to incorporate a flexible phenylamide spacer capable of establishing reversible H-bonding interactions between polymer chains. From a structural standpoint, GIWAXS analyses revealed that the introduction of the **PhAm** motif enhances molecular order, leading to a reduced π–π stacking distance (Fig. 4f). This optimized supramolecular organization translates into a markedly improved mechanical response, as evidenced by pseudo-free tensile tests, in which the **PhAm5:Y7** blend exhibited an increase in the crack-onset strain from 1.8% to 13.8% and a toughness up to 28 times higher than that of the conventional **PM6:Y7** system. Notably, these structural and mechanical enhancements are accompanied by high electronic performance, with PCEs of 17.45% on rigid substrates and 12.73% in fully stretchable devices, which retained 86% of their initial efficiency after 120 stretching cycles. The pioneering work by Diao and co-workers introduces the repurposing of therapeutic agents such as ellipticine as an unconventional yet powerful platform for high-performance, solution-processable OSCs.[139] These molecules feature a highly coplanar π-conjugated backbone decorated with functional groups capable of forming H-bonding networks, which are crucial not only for directing polymorphic self-assembly but also for defining efficient charge-transport pathways. The study demonstrates that H-bonding contributes to electronic coupling in a dual manner: indirectly, by reducing intermolecular distances, and directly, through the delocalization of the electronic wavefunction over the H-bonding motifs themselves. By employing printing techniques that allow precise control over crystalline polymorphism and domain alignment, intrinsic hole mobilities as high as 6.5 $cm^2\ V^{-1}\ s^{-1}$ along the π–π stacking direction and 4.2 $cm^2\ V^{-1}\ s^{-1}$ along the H-bonding network were achieved. These findings provide the first direct experimental evidence of long-range hole transport through H-bond networks in solid-state organic devices and further enable the development of highly sensitive chemical sensors for biomarkers such as ethyl acetate. This behaviour contrasts sharply with that observed in OPV/PDI blends lacking H-bonding, where the strong tendency to form disordered CT complexes leads to unfavourable supramolecular organization and the absence of detectable mobility in FETs. In summary, H-bonding emerges as a uniquely powerful supramolecular tool that programs molecular conformation, hierarchical self-assembly, and nanoscale connectivity, enabling simultaneous optimization of morphology, charge transport, and device stability.

Fluorination effect on organic semiconductors

Beyond supramolecular assembly driven by π–π stacking and H-bonding, chemical fluorination has emerged as a powerful and complementary strategy to modulate molecular conformation, electronic structure, and solid-state packing in organic semiconductors, with profound consequences for charge transport and device stability.[140] Among these strategies, fluorination strategies are one of the most widely used modifications because of the intrinsic properties of fluorine; achieving better co-planarity and extended conjugation, stronger noncovalent interactions, and adjustable LUMO and HOMO levels due to its strong electronegativity and polarized covalent bonds, facilitating electron injection. For instance, Park and co-workers reported controlling ambipolar charge transport in isoindigo (**IIG**)-based polymers through systematically controlling the position of fluorinated moieties placed in bithiophene

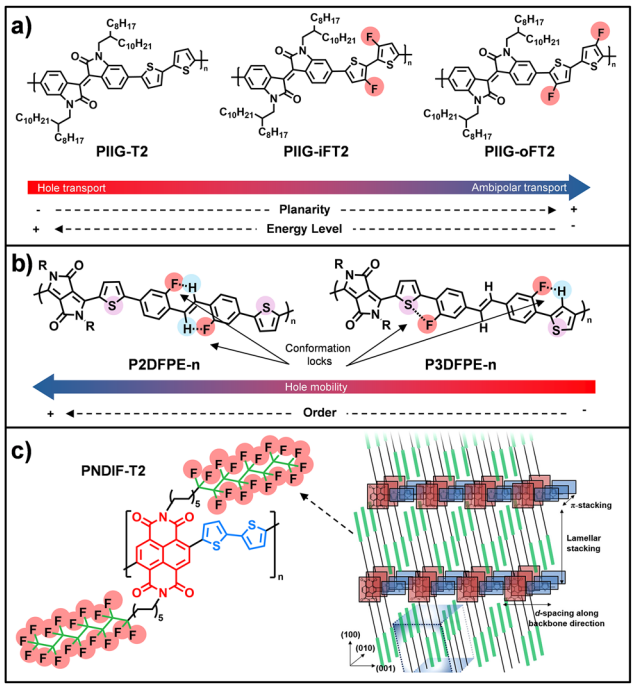

Fig. 5 (a) Chemical structures for **PIIG-T2**, **PIIG-iFT2** and **PIIG-oFT2** and molecular design to control **IIG**-based copolymer polarity by altering fluorine substitution position. (b) Chemical Structures of **P2DFPE** and **P3DFPE** and schematic noncovalent intramolecular interactions. (c) Molecular structure of **PNDIF-T2** and schematic of molecular packing. Adapted from ref. 141, 143, and 144 with permission from Copyright 2019-Wiley-VCH GmbH, 2016, 2015-American Chemical Society, respectively.

linkers.[141] The fluorine atoms were placed either at the outer (**PIIG-oFT2**) or the inner site (**PIIG-iFT2**) of the bithiophene spacers (Fig. 5a). The authors reported that the outer modifications have strong impact in lowering the energy levels and increasing molecular planarity, increasing electron mobility. The analysis of the morphology of the thin films fabricated revealed shorter π–π stacking distance in the case of the incorporation of fluorine atoms in the outer positions of the bithiophenes and a more planar backbone. Gao *et al.* showed the multifluorination effect on **IIG**-based polymers by introducing fluorine atoms into both the **IIG** unit and the bithiophene D unit (**T2**).[142] The authors incorporated perfluorinated **T2(4FT2)** and **TVT(4FTVT)** units, and found out that it is an effective strategy for converting charge polarity from p- to n-type. In this case, close π–π stacking was observed, resulting in improved electron transport (μ_e of **P55** = 4.97 $cm^2 V^{-1} s^{-1}$; μ_e of **P56** = 1.35 $cm^2 V^{-1} s^{-1}$). Additionally, fluorination is a great tool for promoting noncovalent halogen interactions with adjacent atoms, such as C–H···F or S (present in thiophene rings)···F. These interactions largely affected the electronic structure of conjugated polymer backbones, increasing co-planarity. Compounds **P2DFPE-n** and **P3DFPE-n**,[143] lead to different type of intermolecular interactions (Fig. 5b). While **P2DFPE-n** shows F···H–C conformation locks, exhibiting hole mobilities of 1.3–1.5 $cm^2 V^{-1} s^{-1}$, the analogue **P3DFPE-n** displays F···H–C and F···S conformation locks, yielding lower mobilities (0.2–0.4 $cm^2 V^{-1} s^{-1}$). The authors observed with AFM and 2D-GXRD that **P2DFPE-n** is predominantly edge-on oriented, facilitating charge transport and collection, while **P3DFPE-n** adopts random orientation in devices, resulting in lower charge mobility. Alternatively, the fluorination of alkyl chains in polymers and small molecules has been reported to induce crystallinity thanks to supramolecular interactions among the fluorine atoms, reducing conformational freedom, while introducing strong C–F dipoles that promote ordered lamellar packing.[144,145] For example, **PNDIF-T2** and **PNDIF-TVT** showed electron mobility of up to 6.5 $cm^2 V^{-1} s^{-1}$, significantly higher than those of polymers with branched alkyl chains (Fig. 5c). This enhanced side-chain ordering facilitates efficient backbone segregation and π–π stacking, ultimately leading to increased crystallinity. In conclusion, fluorination enables the concurrent optimization of charge transport, environmental stability, and device performance, making it a versatile and powerful strategy for the rational design of high-performance OSCs.

Supramolecular chirality and spin-selective transport in organic electronic devices

Chirality represents a fundamental configurational asymmetry in which an object is not superimposable on its mirror image.[146–148] In molecular chemistry, chirality typically originates from stereogenic centers; however, in systems organized through noncovalent interactions, an additional level of asymmetry emerges in the form of supramolecular chirality.[148] Recent studies indicate that the magnitude and functional impact of this effect do not rely solely on individual molecular chirality, but rather on the global supramolecular organization attained during self-assembly.[149,150] In this hierarchical process, chiral information is transferred and amplified from the molecular to the supramolecular level, extending along a preferred axis and giving rise to complex architectures such as nanohelices, nanotubes or toroidal assemblies.[151–153] These structures display distinctive optical properties, including CD and circularly polarized luminescence (CPL).[154–156] In OSCs, the incorporation of chirality into π-conjugated systems provides an additional level of structural and functional control, as supramolecular organization can enhance charge transport, improve energy conversion efficiency and modulate key photophysical processes such as charge recombination and chiroptical responses. A study led by Aida, involves porphyrin-fullerene dyads, in which molecular chirality was shown to govern both morphology and charge transport, while racemic mixtures form spherical aggregates with poor conductivity, enantiopure systems self-assemble into highly conductive nanofibers, exhibiting markedly enhanced ambipolar mobilities ($\mu_e \approx 0.14$ $cm^2 V^{-1} s^{-1}$ and $\mu_h \approx 0.10$ $cm^2 V^{-1} s^{-1}$ in the absence of an external field).[98,99] Studies led by Würthner have demonstrated that precise control over stereochemical configuration in **DPP**-based semiconductors constitutes a critical design parameter for tuning supramolecular organization and optimizing electronic performance in organic devices. Early investigations revealed that racemic mixtures of 2-ethylhexyl side chains promote highly ordered two-dimensional packing,

yielding hole mobilities of up to 0.7 $cm^2 V^{-1} s^{-1}$ in organic thin-film transistors (**OTFTs**).[157] Remarkably, these values exceed those obtained for polymers bearing linear side chains, despite the isomeric nature of the racemic system. Subsequent isolation of the pure stereoisomers uncovered even more pronounced structure-property relationships.[158] In particular, the (*R*/*S*) isomer exhibits substantially higher hole mobilities, reaching values as high as 3.4 $cm^2 V^{-1} s^{-1}$ in single-crystal field-effect transistors (SCFETs). This enhanced performance is attributed to a markedly more coplanar molecular conformation, which maximizes HOMO orbital overlap and thereby strengthens electronic coupling along the transport direction. From a supramolecular perspective, this favourable architecture is stabilized by a compact network of H-bond interactions, which is absent in the enantiopure counterparts. The latter display increased structural distortion, less efficient packing, and accelerated electronic degradation. Research carried out by Österholm, and co-workers provides valuable insight into how supramolecular chirality can spontaneously emerge from intrinsically achiral components through the strategic use of noncovalent interactions.[159] By designing thiophene-phenylene copolymers, the study demonstrates that incorporation of a bithiophene unit into the **TPT-2T** (Fig. 6a) system induces, upon thermal annealing, the formation of a helicoidal conformation, in stark contrast to the planar and highly crystalline morphology adopted by the **TPT-T** analogue (Fig. 6a). This emergent chirality is stabilized by a cooperative network of weak intramolecular interactions (S···O, O···H–C, and S···H–C), which restrict backbone rotation and generate moderate torsional energy barriers (~2.9 kcal mol^{-1}), favouring helical winding over planar conformations. The resulting chiral packing was confirmed by circular dichroism (CD) spectroscopy, evidencing that the structural asymmetry arises as a collective property of the supramolecular assembly rather than from molecular stereogenic elements. From an electronic perspective, this nanomolecular organization has a direct impact on the performance of OFETs. Although the helicoidal torsion limits charge-carrier mobility relative to fully planar systems, the chiral polymer exhibits defect-free and homogeneous charge transport, characterized by a near-zero threshold voltage, indicative of a highly optimized semiconductor-dielectric interface. Studies led by Wei and collaborators have further demonstrated how chiral supramolecular organization dictates charge transport and optoelectronic functionality in advanced devices. In an investigation of the fused-ring electron acceptor **BTP-4F**, replacing racemic side chains with enantiopure counterparts was shown to induce a profound transformation in solid-state packing.[160] Whereas the racemic material forms interpenetrated 3D networks with microribbon-like morphology, the enantiopure systems self-assemble into a unique quasi-2D supramolecular organization, characterized by interwoven molecules adopting helicoidal conformations of opposite handedness. This arrangement results in pronounced electronic anisotropy, with electron mobilities reaching up to 0.44 $cm^2 V^{-1} s^{-1}$ along the preferred growth direction-among the highest values reported for intrinsically chiral organic semiconductors. In a subsequent advance, Wei explored bulk heterojunctions composed of the chiral donor **DPP6T** and the achiral acceptor **$PC_{61}BM$**, demonstrating that the density of chiral centers in the side chains constitutes a critical parameter for supramolecular organization (Fig. 6b).[161] This mesoscopically induced chirality enabled efficient detection of circularly polarized light, yielding photocurrent dissymmetry factors as high as 0.17 and evidencing significantly enhanced charge separation and collection. The studies by Amabilino provide a representative example of how molecular chirality and symmetry act as key parameters in modulating the supramolecular self-assembly of DPP-based chromophores.[162] In bulk heterojunctions composed of a **chiral bis-DPP** as **D** molecule and the achiral **ITIC-4F** as A derivative, it was shown that the A strongly perturbs the chiral organization of the D component in a thickness-dependent manner. Mueller matrix polarimetry using synchrotron radiation revealed that this supramolecular reorganization induces changes in both the magnitude and sign of the optical activity across the active layer (Fig. 6).

These structural variations directly impact device performance, leading to an external quantum efficiency (EQE) that is selective toward the handedness of circularly polarized light (LCP/RCP).[163] A key advance associated with chirality in supramolecular systems is the chirality-induced spin selectivity (CISS) effect.[164,165] This phenomenon describes how electronic transport through chiral structures becomes intrinsically spin-dependent, such that electrons with a given spin orientation are preferentially transmitted over their opposite counterparts. As

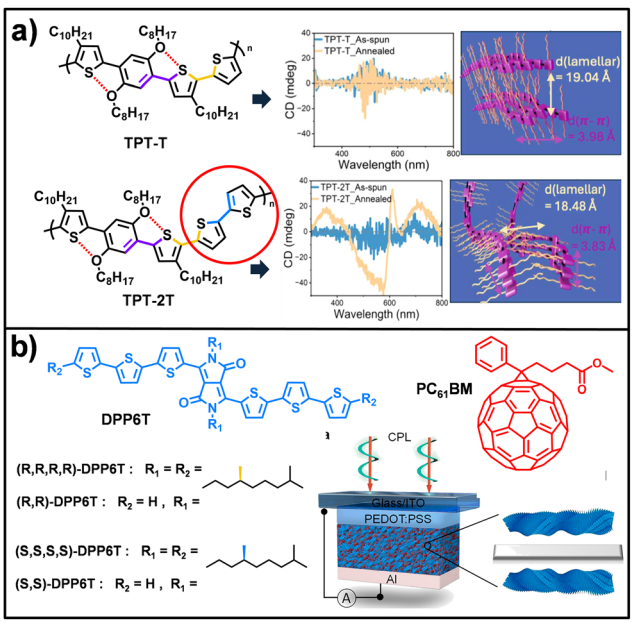

Fig. 6 (a) Molecular structure of **TPT-T** and **TPT-2T** and CD spectra and their structural illustrations. **TPT-T** shows zero cotton effect, confirming its achiral nature while **TPT-2T** exhibits circular dichroism activity due to the formation of chiral mesophases during annealing. (b) Molecular structure of **DPP6T** and **$PC_{61}BM$** and configuration of chiral OSCs. Adapted from ref. 159 and 162 with permission from Copyright 2025 and 2022-American Chemical Society, respectively.

an electron propagates through the helicoidal electrostatic potential of a chiral molecule or supramolecular assembly, an effective coupling between its linear momentum and spin arises, acting as an internal magnetic field along the transport pathway.[166] The incorporation of the CISS effect into supramolecular organic semiconductors has opened new opportunities in organic spintronics and optoelectronics, as chiral architectures can function as highly efficient spin filters without the need for ferromagnetic electrodes.[153,167] This spin selectivity suppresses electronic backscattering and charge recombination, thereby promoting long-range charge-transfer processes and improving device performance relative to achiral systems.[166,168] The work led by Geerts and Schweicher represents a major milestone in the integration of CISS effect into molecular electronics, reporting the first OFET whose current can be fully and reversibly switched by inversion of an external magnetic field.[169] In this study, enantiopure semiconductors based on **DNTT** core were designed and functionalized with chiral alkyl side chains, inducing an asymmetric herringbone crystal packing (Fig. 7a). In devices employing conventional gold contacts, both enantiomers exhibit comparable charge-carrier mobilities, indicating that chirality alone does not significantly influence charge transport in the absence of spin polarization. In contrast, the introduction of ferromagnetic Ni/Au contacts reveals a pronounced dependence of the electrical response on both molecular handedness and magnetization direction. Specifically, OFETs based on **(*S*)-DNTT** conduct current only when the magnetic field is parallel to the direction of hole transport, whereas **(*R*)-DNTT** devices display conduction exclusively in the antiparallel configuration, enabling binary (on/off) control of the channel current. Research led by Diao and Sun reported the first observation of the inverse chirality-induced spin selectivity (ICISS) effect in assemblies of organic polymers.[170] In this work, an initially achiral π-conjugated polymer, **PII2T**, was employed, which acquires supramolecular chirality in the form of helicoidal nanofibers through a solution-based printing process that enables precise control over the handedness (*R* or *S*) and the helical pitch of thin films (Fig. 7b). To probe the ICISS effect, devices based on spin-pumping were developed, in which a spin current is injected from a ferromagnetic $Ni_{81}Fe_{19}$ layer into the chiral polymer and subsequently converted into a longitudinal charge current. The results showed that the generated voltage reverses its sign upon inversion of the film chirality, demonstrating that spin-to-charge conversion is governed exclusively by the supramolecular chiral structure and by an unconventional spin-orbit coupling. A particularly noteworthy outcome was the observation of exceptionally long spin relaxation times, reaching up to 2.5 ns when spin propagation occurs parallel to the chiral axis of the nanofibers, far exceeding the values typically reported for conventional organic systems.[171] Overall, supramolecular chirality introduces an additional functional dimension in organic electronics, where chiral self-assembly governs charge transport anisotropy, chiroptical response, and spin-selective processes through the CISS effect.

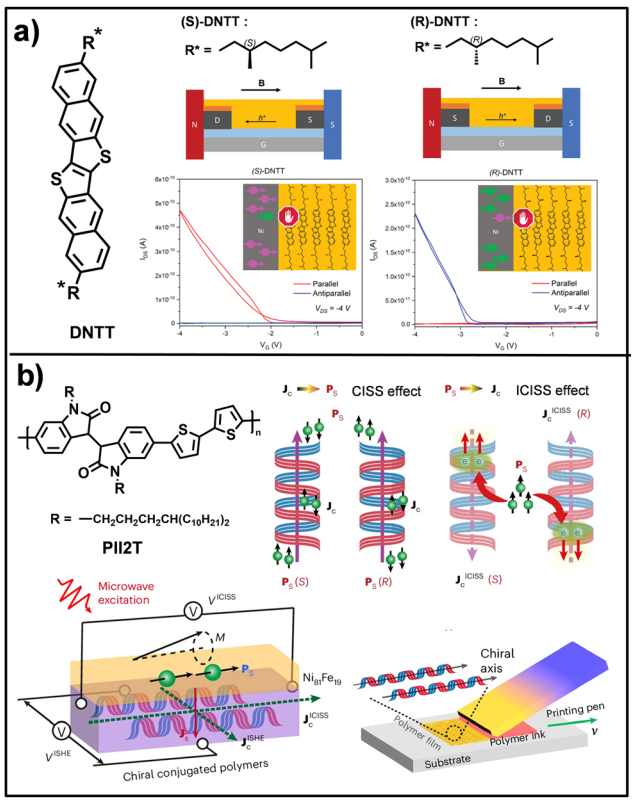

Fig. 7 (a) Molecular structure of **DNTT** and geometry of a BGBC device with ferromagnetic electrodes. Transfer curves (bottom) in saturation regime (V_d = −4 V) of **(*R*)-DNTT** (right) and **(*S*)-DNTT** (left) in a parallel or antiparallel magnetic field. (b) Molecular structure of **PII2T**. Representation of the CISS/ICISS effect and the flow of charge current. Schematic illustration of the ISHE and ICISS measurements in the device *via* the spin-pumping method under microwave excitation (bottom left). Schematic diagram of helical structure accessed *via* blade printing (bottom, right). Adapted from ref. 169 and 170 with permission from Copyright 2023-Wiley-VCH GmbH and 2024-Springer Nature, respectively.

Other noncovalent interactions beyond H-bonding and π–π stacking

Beyond classical interactions such as H-bonding and π–π stacking, supramolecular electronics has incorporated a broader repertoire of noncovalent forces that enable even finer control over molecular organization, interfacial properties, and device performance.[58,59,68] Halogen bonding has emerged as a particularly attractive design tool owing to its high directionality and hydrophobic character.[71,172] Specific N···I interactions have been shown to generate 2D organic cocrystals with highly defined morphologies, capable of guiding directional photon transport and enabling microscale optical logic functions.[173] In thiophene-based semiconductors, halogen-halogen and halogen-H interactions stabilize ordered monolayers at liquid–solid interfaces, where halogen-induced ordering correlates directly with hole mobility in OFET devices.[174] Halogen bonding has also been exploited to develop piezochromic supramolecular assemblies for applications in haptic memories and sensors.[175]

Chalcogen bonding has likewise emerged as an effective noncovalent interaction for modulating both molecular conformation and solid-state packing in organic semiconductors, particularly in systems rich in group 16 heteroatoms. Recent studies demonstrate that nonbonding X···S interactions (X = O, S, Se) can induce highly efficient intramolecular conformational locking, promoting backbone planarization and enhanced charge transport.[176] In bithiophene derivatives, the incorporation of heavier chalcogens into side chains proves especially effective, with selenium-based systems achieving hole mobilities exceeding 4 $cm^2\ V^{-1}\ s^{-1}$, emphasising that conformational control *via* substituents can be as impactful as direct modification of the aromatic core.[177]

Dipole–dipole interactions have further emerged as a key tool for modulating the optical and emissive properties of OSCs. Studies on *p*-phenylene vinylene oligomers have shown that systematic modification of terminal groups allows precise tuning of the molecular dipole moment, directly affecting supramolecular aggregation and solute-solvent interactions. These effects translate into extreme solvatochromism and pronounced evolution of emissive properties with direct implications for OLED performance.[178]

Quadrupolar interactions have been identified as a critical factor in tuning energy levels in OSCs by generating permanent electrostatic shifts that depend strongly on molecular orientation and supramolecular packing. In zinc phthalocyanines, the ionization energy has been shown to vary linearly with the component of the molecular quadrupole moment perpendicular to the π-plane, with differences of up to ~0.4 eV observed between edge-on and face-on orientations. This quadrupolar control enables fine tuning of charge-transfer state energies and reduction of dissociation barriers in organic solar cells.[179]

Finally, metal-ligand coordination represents one of the most robust noncovalent interactions, combining high binding energies with structural reversibility. This strategy enables hierarchical self-assembly into well-defined architectures ranging from 2D to 3D motifs, which can further reorganize into responsive nanofibers or supramolecular networks. Metal-ligand coordination thus constitutes a powerful supramolecular tool for modulating charge transport and photoresponse in organic devices by coupling strong interactions with precise geometrical control.[122] In optoelectronic applications, coordinated metal complexes have demonstrated outstanding performance in OLEDs, as well as advanced functionalities such as vapochromism arising from environmentally sensitive metallophilic interactions.[180] A notable example is the development of flexible organic phototransistors sensitized with ruthenium complexes, where functionalization of an *n*-type semiconductor with a Ru-complex enables highly efficient metal-ligand charge transfer.[181] Less conventional noncovalent interactions, such as the ones here presented, expand the supramolecular toolbox, enabling precise control over molecular orientation, energy landscapes, and emergent optoelectronic functionality.

Outlook, future perspectives and conclusions

The body of work discussed in this review demonstrates that supramolecular chemistry has transitioned from a descriptive framework of molecular aggregation to a powerful design tool for organic electronic devices. Yet, despite impressive demonstrations of high mobility, enhanced stability, and morphology control, the field remains largely empirical. The next phase of supramolecular organic electronics must therefore move beyond incremental performance gains toward predictive and programmable materials engineering.

A central challenge lies in achieving quantitative and reproducible control over supramolecular assembly during device processing. While numerous examples demonstrate improved charge-carrier mobility or photovoltaic efficiency, the translation of molecular design into macroscopic device function remains highly sensitive to processing history, solvent environment, and kinetic trapping. Future progress will require the development of standardized structural descriptors, such as stacking coherence length, energetic disorder parameters, hydrogen-bond density, and domain connectivity metrics, that directly correlate supramolecular order with device-level observables. The integration of multiscale modelling, advanced scattering techniques, and data-driven approaches will be essential to bridge molecular structure with mesoscale morphology and electronic function.

In this context, ''continued improvement'' should be defined not only qualitatively but quantitatively. Supramolecular strategies should aim to routinely deliver charge-carrier mobilities exceeding 10 $cm^2\ V^{-1}\ s^{-1}$ under ambient conditions,[9] certified power conversion efficiencies surpassing 20% with minimized non-radiative losses,[126] and operational lifetimes beyond 10^4 hours without morphological degradation.[182] More importantly, these metrics must be achieved with reproducibility and scalability, demonstrating that supramolecular design offers advantages beyond those accessible through purely covalent structural modification.

A transformative direction for the field involves shifting from the elimination of disorder to its rational programming. Rather than seeking perfectly crystalline order, supramolecular systems offer the possibility of defect-tolerant and dynamically adaptive networks in which reversible noncovalent interactions enable self-correction and morphological stabilization under operational stress. Designing materials in which hydrogen bonding, π–π stacking, halogen bonding, and dipolar interactions act cooperatively and hierarchically may enable three-dimensional electronically percolated architectures that overcome the limitations of predominantly one-dimensional stacking motifs.

Beyond charge transport optimization, supramolecular organization opens avenues toward emergent functionalities. The incorporation of chirality, for example, should not be viewed merely as an additional structural parameter, but as a gateway to spin-selective transport and quantum-coherent phenomena in organic solids. Bridging molecular-scale CISS effects with

device-scale architectures operating at room temperature remains an open challenge with profound implications for organic spintronics. Similarly, dynamic supramolecular networks capable of adaptive reconfiguration, self-healing, or stimuli responsiveness may enable mechanically resilient and multifunctional electronic systems.

Finally, the technological relevance of supramolecular electronics will depend on its compatibility with scalable manufacturing. Synthetic accessibility, cost-effective building blocks, and robustness under large-area printing must be considered as integral design constraints rather than secondary considerations. The maturation of supramolecular electronics will therefore require convergence between synthetic chemistry, device physics, computational modelling, and process engineering.

In summary, noncovalent interactions should no longer be regarded as auxiliary forces supporting organic semiconductor performance. They constitute precision engineering tools capable of programming molecular architecture, mesoscale morphology, and emergent device functionality. As predictive design principles become established, supramolecular chemistry can redefine the conceptual foundation of next-generation organic electronic technologies.

Author contributions

ARC supervised the work, secured funding, and oversaw the writing and finalisation of the manuscript. MGS led the writing of the manuscript and supervised the preparation of figures. XW was responsible for figure preparation. KIH contributed to and supervised the fluorination-related aspects of the work. RGN supervised the device-related work. All authors contributed to the writing and editing of the manuscript and approved the final version.

Conflicts of interest

There are no conflicts to declare.

Data availability

All data discussed in this review are available in the cited literature.

Acknowledgements

The authors thank support from the Spanish Ministry of Science and Innovation and the Spanish State Research Agency (Project ATR2024-154740).

Notes and references

1 M. Madhu, R. Ramakrishnan, V. Vijay and M. Hariharan, *Chem. Rev.*, 2021, **121**, 8234–8284.
2 D. Gust, T. A. Moore and A. L. Moore, *Acc. Chem. Res.*, 2001, **34**, 40–48.
3 L. Hammarström and S. Hammes-Schiffer, *Acc. Chem. Res.*, 2009, **42**, 1859–1860.
4 G. D. Scholes, G. R. Fleming, A. Olaya-Castro and R. van Grondelle, *Nat. Chem.*, 2011, **3**, 763–774.
5 J. Follana-Berná, A. Dawson, R. R. Kaswan, S. Seetharaman, P. A. Karr, Á. Sastre-Santos and F. D'Souza, *J. Phys. Chem. A*, 2023, **127**, 6191–6203.
6 C. W. Tang and S. A. VanSlyke, *Appl. Phys. Lett.*, 1987, **51**, 913–915.
7 M. Fahlman, S. Fabiano, V. Gueskine, D. Simon, M. Berggren and X. Crispin, *Nat. Rev. Mater.*, 2019, **4**, 627–650.
8 P. Friederich, A. Fediai, S. Kaiser, M. Konrad, N. Jung and W. Wenzel, *Adv. Mater.*, 2019, **31**, 1808256.
9 M. Yuan, Y. Qiu, H. Gao, J. Feng, L. Jiang and Y. Wu, *J. Am. Chem. Soc.*, 2024, **146**, 7885–7904.
10 W. Jin, Y. Yamamoto, T. Fukushima, N. Ishii, J. Kim, K. Kato, M. Takata and T. Aida, *J. Am. Chem. Soc.*, 2008, **130**, 9434–9440.
11 W. Zhang, W. Jin, T. Fukushima, A. Saeki, S. Seki and T. Aida, *Science*, 2011, **334**, 340–343.
12 J. H. Burroughes, D. D. C. Bradley, A. R. Brown, R. N. Marks, K. Mackay, R. H. Friend, P. L. Burns and A. B. Holmes, *Nature*, 1990, **347**, 539–541.
13 A. P. Kulkarni, C. J. Tonzola, A. Babel and S. A. Jenekhe, *Chem. Mater.*, 2004, **16**, 4556–4573.
14 H. Uoyama, K. Goushi, K. Shizu, H. Nomura and C. Adachi, *Nature*, 2012, **492**, 234–238.
15 T.-H. Han, Y. Lee, M.-R. Choi, S.-H. Woo, S.-H. Bae, B. H. Hong, J.-H. Ahn and T.-W. Lee, *Nat. Photonics*, 2012, **6**, 105–110.
16 H. Zhang, D.-Q. Lin, W. Liu, Y.-C. Wang, Z.-X. Li, D. Jin, J. Wang, X.-W. Zhang, L. Huang, S.-S. Wang, C.-X. Xu, Y.-H. Kan and L.-H. Xie, *Adv. Mater. Interfaces*, 2022, **9**, 2200194.
17 X. Yan, H. Peng, Y. Xiang, J. Wang, L. Yu, Y. Tao, H. Li, W. Huang and R. Chen, *Small*, 2022, **18**, 2104073.
18 H. Hoppe and N. S. Sariciftci, *J. Mater. Res.*, 2004, **19**, 1924–1945.
19 J. Y. Kim, K. Lee, N. E. Coates, D. Moses, T.-Q. Nguyen, M. Dante and A. J. Heeger, *Science*, 2007, **317**, 222–225.
20 I. Hirao, M. Kimoto and R. Yamashige, *Acc. Chem. Res.*, 2012, **45**, 2055–2065.
21 F. Würthner, Z. Chen, F. J. M. Hoeben, P. Osswald, C.-C. You, P. Jonkheijm, J. V. Herrikhuyzen, A. P. H. J. Schenning, P. P. A. M. van der Schoot, E. W. Meijer, E. H. A. Beckers, S. C. J. Meskers and R. A. J. Janssen, *J. Am. Chem. Soc.*, 2004, **126**, 10611–10618.
22 Y. Wang, A. Vogel, M. Sachs, R. S. Sprick, L. Wilbraham, S. J. A. Moniz, R. Godin, M. A. Zwijnenburg, J. R. Durrant, A. I. Cooper and J. Tang, *Nat. Energy*, 2019, **4**, 746–760.
23 C. Zhong, Y. Yan, Q. Peng, Z. Zhang, T. Wang, X. Chen, J. Wang, Y. Wei, T. Yang and L. Xie, *Nanomaterials*, 2023, **13**, 1750.
24 J. L. Delgado, P.-A. Bouit, S. Filippone, M. Á. Herranz and N. Martín, *Chem. Commun.*, 2010, **46**, 4853–4865.
25 Y. He and Y. Li, *Phys. Chem. Chem. Phys.*, 2011, **13**, 1970–1983.
26 C. D. Dimitrakopoulos and P. R. L. Malenfant, *Adv. Mater.*, 2002, **14**, 99–117.
27 H. Sirringhaus, *Adv. Mater.*, 2005, **17**, 2411–2425.
28 H. H. Choi, K. Cho, C. D. Frisbie, H. Sirringhaus and V. Podzorov, *Nat. Mater.*, 2018, **17**, 2–7.
29 W. Wu, Y. Liu and D. Zhu, *Chem. Soc. Rev.*, 2010, **39**, 1489–1502.
30 C. Wang, H. Dong, W. Hu, Y. Liu and D. Zhu, *Chem. Rev.*, 2012, **112**, 2208–2267.
31 H. Wang and C. Yu, *Joule*, 2019, **3**, 53–80.
32 Z. B. Henson, K. Müllen and G. C. Bazan, *Nat. Chem.*, 2012, **4**, 699–704.
33 F. Liu, C. Wang, J. K. Baral, L. Zhang, J. J. Watkins, A. L. Briseno and T. P. Russell, *J. Am. Chem. Soc.*, 2013, **135**, 19248–19259.
34 M. Mas-Torrent and C. Rovira, *Chem. Rev.*, 2011, **111**, 4833–4856.
35 H. Li, P. Shao, S. Chen, G. Li, X. Feng, X. Chen, H.-J. Zhang, J. Lin and Y.-B. Jiang, *J. Am. Chem. Soc.*, 2020, **142**, 3712–3717.
36 G. Koshkakaryan, L. M. Klivansky, D. Cao, M. Snauko, S. J. Teat, J. O. Struppe and Y. Liu, *J. Am. Chem. Soc.*, 2009, **131**, 2078–2079.
37 F. J. M. Hoeben, P. Jonkheijm, E. W. Meijer and A. P. H. J. Schenning, *Chem. Rev.*, 2005, **105**, 1491–1546.
38 T. Setzer, P. Friederich, V. Meded, W. Wenzel, C. Lennartz and A. Dreuw, *ChemPhysChem*, 2018, **19**, 2961–2966.
39 U. Würfel, D. Neher, A. Spies and S. Albrecht, *Nat. Commun.*, 2015, **6**, 6951.
40 J. Benduhn, K. Tvingstedt, F. Piersimoni, S. Ullbrich, Y. Fan, M. Tropiano, K. A. McGarry, O. Zeika, M. K. Riede, C. J. Douglas,

S. Barlow, S. R. Marder, D. Neher, D. Spoltore and K. Vandewal, *Nat. Energy*, 2017, **2**, 17053.
41 X. Lin, B. Wegner, K. M. Lee, M. A. Fusella, F. Zhang, K. Moudgil, B. P. Rand, S. Barlow, S. R. Marder, N. Koch and A. Kahn, *Nat. Mater.*, 2017, **16**, 1209–1215.
42 D. Venkateshvaran, M. Nikolka, A. Sadhanala, V. Lemaur, M. Zelazny, M. Kepa, M. Hurhangee, A. J. Kronemeijer, V. Pecunia, I. Nasrallah, I. Romanov, K. Broch, I. McCulloch, D. Emin, Y. Olivier, J. Cornil, D. Beljonne and H. Sirringhaus, *Nature*, 2014, **515**, 384–388.
43 S. Fratini, M. Nikolka, A. Salleo, G. Schweicher and H. Sirringhaus, *Nat. Mater.*, 2020, **19**, 491–502.
44 J. Ko, R. Berger, H. Lee, H. Yoon, J. Cho and K. Char, *Chem. Soc. Rev.*, 2021, **50**, 3585–3628.
45 J. Yan, E. Rezasoltani, M. Azzouzi, F. Eisner and J. Nelson, *Nat. Commun.*, 2021, **12**, 3642.
46 O. J. Sandberg, C. Kaiser, S. Zeiske, N. Zarrabi, S. Gielen, W. Maes, K. Vandewal, P. Meredith and A. Armin, *Nat. Photonics*, 2023, **17**, 368–374.
47 H. Bronstein, C. B. Nielsen, B. C. Schroeder and I. McCulloch, *Nat. Rev. Chem.*, 2020, **4**, 66–77.
48 H. Spanggaard and F. C. Krebs, *Sol. Energy Mater. Sol. Cells*, 2004, **83**, 125–146.
49 B. C. Thompson and J. M. J. Fréchet, *Angew. Chem., Int. Ed.*, 2008, **47**, 58–77.
50 T. L. Benanti and D. Venkataraman, *Photosynth. Res.*, 2006, **87**, 73–81.
51 P. A. Korevaar, T. F. A. de Greef and E. W. Meijer, *Chem. Mater.*, 2014, **26**, 576–586.
52 P. M. Beaujuge and J. M. J. Fréchet, *J. Am. Chem. Soc.*, 2011, **133**, 20009–20029.
53 M. Graetzel, R. A. J. Janssen, D. B. Mitzi and E. H. Sargent, *Nature*, 2012, **488**, 304–312.
54 J. Mei, Y. Diao, A. L. Appleton, L. Fang and Z. Bao, *J. Am. Chem. Soc.*, 2013, **135**, 6724–6746.
55 R. Noriega, J. Rivnay, K. Vandewal, F. P. V. Koch, N. Stingelin, P. Smith, M. F. Toney and A. Salleo, *Nat. Mater.*, 2013, **12**, 1038–1044.
56 C. M. Proctor, A. S. Kher, J. A. Love, Y. Huang, A. Sharenko, G. C. Bazan and T.-Q. Nguyen, *Adv. Energy Mater.*, 2016, **6**, 1502285.
57 E. W. Meijer and A. P. H. J. Schenning, *Nature*, 2002, **419**, 353–354.
58 H. Chen and J. Fraser Stoddart, *Nat. Rev. Mater.*, 2021, **6**, 804–828.
59 Y. Yao, L. Zhang, E. Orgiu and P. Samorì, *Adv. Mater.*, 2019, **31**, 1900599.
60 N. Nerngchamnong, L. Yuan, D.-C. Qi, J. Li, D. Thompson and C. A. Nijhuis, *Nat. Nanotechnol.*, 2013, **8**, 113–118.
61 N. T. Shewmon, D. L. Watkins, J. F. Galindo, R. B. Zerdan, J. Chen, J. Keum, A. E. Roitberg, J. Xue and R. K. Castellano, *Adv. Funct. Mater.*, 2015, **25**, 5166–5177.
62 A. J. Fleming, J. N. Coleman, A. B. Dalton, A. Fechtenkötter, M. D. Watson, K. Müllen, H. J. Byrne and W. J. Blau, *J. Phys. Chem. B*, 2003, **107**, 37–43.
63 Z. Chen, A. Lohr, C. R. Saha-Moller and F. Wurthner, *Chem. Soc. Rev.*, 2009, **38**, 564–584.
64 P. K. Baruah and S. Khan, *RSC Adv.*, 2013, **3**, 21202–21217.
65 M. J. Krische and J.-M. Lehn, in *Molecular Self-Assembly Organic Versus Inorganic Approaches*, ed. M. Fuiita, Springer Berlin Heidelberg, Berlin, Heidelberg, 2000, pp. 3–29, DOI: 10.1007/3-540-46591-X_1.
66 J. D. Bernal, H. D. Megaw and R. H. Fowler, *Proc. R. Soc. A*, 1935, **151**, 384–420.
67 M. L. Huggins, *J. Org. Chem.*, 1936, **01**, 407–456.
68 D. Lombardo, P. Calandra, L. Pasqua and S. Magazù, *Materials*, 2020, **13**, 1048.
69 J. D. Badjić, A. Nelson, S. J. Cantrill, W. B. Turnbull and J. F. Stoddart, *Acc. Chem. Res.*, 2005, **38**, 723–732.
70 O. Dumele, J. Chen, J. V. Passarelli and S. I. Stupp, *Adv. Mater.*, 2020, **32**, 1907247.
71 E. Busseron, Y. Ruff, E. Moulin and N. Giuseppone, *Nanoscale*, 2013, **5**, 7098–7140.
72 T. Aida, E. W. Meijer and S. I. Stupp, *Science*, 2012, **335**, 813–817.
73 F. Tantakitti, J. Boekhoven, X. Wang, R. V. Kazantsev, T. Yu, J. Li, E. Zhuang, R. Zandi, J. H. Ortony, C. J. Newcomb, L. C. Palmer, G. S. Shekhawat, M. O. de la Cruz, G. C. Schatz and S. I. Stupp, *Nat. Mater.*, 2016, **15**, 469–476.
74 B. Su, S. Wang, J. Ma, Y. Wu, X. Chen, Y. Song and L. Jiang, *Adv. Mater.*, 2012, **24**, 559.
75 M. González-Sánchez, J. S. Valera, J. Veiga-Herrero, P. B. Chamorro, F. Aparicio and D. González-Rodríguez, *Chem. Soc. Rev.*, 2025, **54**, 5657–5697.
76 Y. Yamamoto, T. Fukushima, Y. Suna, N. Ishii, A. Saeki, S. Seki, S. Tagawa, M. Taniguchi, T. Kawai and T. Aida, *Science*, 2006, **314**, 1761–1764.
77 J. Xu, H.-C. Wu, C. Zhu, A. Ehrlich, L. Shaw, M. Nikolka, S. Wang, F. Molina-Lopez, X. Gu, S. Luo, D. Zhou, Y.-H. Kim, G.-J. N. Wang, K. Gu, V. R. Feig, S. Chen, Y. Kim, T. Katsumata, Y.-Q. Zheng, H. Yan, J. W. Chung, J. Lopez, B. Murmann and Z. Bao, *Nat. Mater.*, 2019, **18**, 594–601.
78 Z. Wang, M. Si, J. Han, Y. Shen, G. Yin, K. Yin, P. Xiao and T. Chen, *Angew. Chem., Int. Ed.*, 2025, **64**, e202416095.
79 M. González-Sánchez, A. M. Garcia, J. S. Valera, A. M. Rodríguez, J. Cabanillas-González, P. Prieto and D. González-Rodríguez, *Chem. Sci.*, 2026, **17**, 2386–2394.
80 L. Brunsveld, B. J. B. Folmer, E. W. Meijer and R. P. Sijbesma, *Chem. Rev.*, 2001, **101**, 4071–4098.
81 T. F. A. De Greef, M. M. J. Smulders, M. Wolffs, A. P. H. J. Schenning, R. P. Sijbesma and E. W. Meijer, *Chem. Rev.*, 2009, **109**, 5687–5754.
82 C. Frieden, *Protein Sci.*, 2007, **16**, 2334–2344.
83 A. Sarkar, T. Behera, R. Sasmal, R. Capelli, C. Empereur-mot, J. Mahato, S. S. Agasti, G. M. Pavan, A. Chowdhury and S. J. George, *J. Am. Chem. Soc.*, 2020, **142**, 11528–11539.
84 L. Zang, Y. Che and J. S. Moore, *Acc. Chem. Res.*, 2008, **41**, 1596–1608.
85 W. Pisula, X. Feng and K. Müllen, *Adv. Mater.*, 2010, **22**, 3634–3649.
86 G. E. J. Hicks, S. Li, N. K. Obhi, C. N. Jarrett-Wilkins and D. S. Seferos, *Adv. Mater.*, 2021, **33**, 2006287.
87 R. González-Núñez, G. Martinez, N. R. Avila-Rovelo, K.-I. Hong, A. Ruiz-Carretero and R. Ponce Ortiz, *J. Mater. Chem. C*, 2024, **12**, 18264–18273.
88 A. P. H. J. Schenning and E. W. Meijer, *Chem. Commun.*, 2005, 3245–3258, DOI: 10.1039/B501804H.
89 J. Wu, M. D. Watson, L. Zhang, Z. Wang and K. Müllen, *J. Am. Chem. Soc.*, 2004, **126**, 177–186.
90 J. M. Mativetsky, M. Kastler, R. C. Savage, D. Gentilini, M. Palma, W. Pisula, K. Müllen and P. Samori, *Adv. Funct. Mater.*, 2009, **19**, 2486–2494.
91 M. D. Watson, A. Fechtenkötter and K. Müllen, *Chem. Rev.*, 2001, **101**, 1267–1300.
92 C. D. Simpson, J. Wu, M. D. Watson and K. Müllen, *J. Mater. Chem.*, 2004, **14**, 494–504.
93 R. J. Bushby and O. R. Lozman, *Curr. Opin. Solid State Mater. Sci.*, 2002, **6**, 569–578.
94 K. Müllen and J. P. Rabe, *Acc. Chem. Res.*, 2008, **41**, 511–520.
95 A. M. V. D. Craats, J. M. Warman, A. Fechtenkötter, J. D. Brand, M. A. Harbison and K. Müllen, *Adv. Mater.*, 1999, **11**, 1469–1472.
96 J. Wu, W. Pisula and K. Müllen, *Chem. Rev.*, 2007, **107**, 718–747.
97 W.-S. Li, Y. Yamamoto, T. Fukushima, A. Saeki, S. Seki, S. Tagawa, H. Masunaga, S. Sasaki, M. Takata and T. Aida, *J. Am. Chem. Soc.*, 2008, **130**, 8886–8887.
98 Y. Hizume, K. Tashiro, R. Charvet, Y. Yamamoto, A. Saeki, S. Seki and T. Aida, *J. Am. Chem. Soc.*, 2010, **132**, 6628–6629.
99 R. Charvet, Y. Yamamoto, T. Sasaki, J. Kim, K. Kato, M. Takata, A. Saeki, S. Seki and T. Aida, *J. Am. Chem. Soc.*, 2012, **134**, 2524–2527.
100 A. Saeki, Y. Koizumi, T. Aida and S. Seki, *Acc. Chem. Res.*, 2012, **45**, 1193–1202.
101 S. M. Mickley Conron, L. E. Shoer, A. L. Smeigh, A. B. Ricks and M. R. Wasielewski, *J. Phys. Chem. B*, 2013, **117**, 2195–2204.
102 P. E. Hartnett, S. M. Dyar, E. A. Margulies, L. E. Shoer, A. W. Cook, S. W. Eaton, T. J. Marks and M. R. Wasielewski, *Chem. Sci.*, 2015, **6**, 402–411.
103 J. E. Bullock, R. Carmieli, S. M. Mickley, J. Vura-Weis and M. R. Wasielewski, *J. Am. Chem. Soc.*, 2009, **131**, 11919–11929.
104 A. Mandal, J. D. Schultz, Y.-L. Wu, A. F. Coleman, R. M. Young and M. R. Wasielewski, *J. Phys. Chem. Lett.*, 2019, **10**, 3509–3515.

105 T. van der Boom, R. T. Hayes, Y. Zhao, P. J. Bushard, E. A. Weiss and M. R. Wasielewski, *J. Am. Chem. Soc.*, 2002, **124**, 9582–9590.
106 J. L. Logsdon, P. E. Hartnett, J. N. Nelson, M. A. Harris, T. J. Marks and M. R. Wasielewski, *ACS Appl. Mater. Interfaces*, 2017, **9**, 33493–33503.
107 B. Rybtchinski, L. E. Sinks and M. R. Wasielewski, *J. Phys. Chem. A*, 2004, **108**, 7497–7505.
108 H. T. Black, N. Yee, Y. Zems and D. F. Perepichka, *Chem. – Eur. J.*, 2016, **22**, 17251–17261.
109 H. Kar and S. Ghosh, *Isr. J. Chem.*, 2019, **59**, 881–891.
110 Z. Xiao, T. Duan, H. Chen, K. Sun and S. Lu, *Sol. Energy Mater. Sol. Cells*, 2018, **182**, 1–13.
111 D.-W. Zhang, X. Zhao, J.-L. Hou and Z.-T. Li, *Chem. Rev.*, 2012, **112**, 5271–5316.
112 L. J. Prins, D. N. Reinhoudt and P. Timmerman, *Angew. Chem., Int. Ed.*, 2001, **40**, 2382–2426.
113 R. P. Sijbesma and E. W. Meijer, *Chem. Commun.*, 2003, 5–16, DOI: 10.1039/B205873C.
114 J. L. Sessler, C. M. Lawrence and J. Jayawickramarajah, *Chem. Soc. Rev.*, 2007, **36**, 314–325.
115 E. D. Głowacki, M. Irimia-Vladu, M. Kaltenbrunner, J. Gsiorowski, M. S. White, U. Monkowius, G. Romanazzi, G. P. Suranna, P. Mastrorilli, T. Sekitani, S. Bauer, T. Someya, L. Torsi and N. S. Sariciftci, *Adv. Mater.*, 2013, **25**, 1563–1569.
116 H. T. Black and D. F. Perepichka, *Angew. Chem., Int. Ed.*, 2014, **53**, 2138–2142.
117 A. S. Tayi, A. K. Shveyd, A. C. H. Sue, J. M. Szarko, B. S. Rolczynski, D. Cao, T. J. Kennedy, A. A. Sarjeant, C. L. Stern, W. F. Paxton, W. Wu, S. K. Dey, A. C. Fahrenbach, J. R. Guest, H. Mohseni, L. X. Chen, K. L. Wang, J. F. Stoddart and S. I. Stupp, *Nature*, 2012, **488**, 485–489.
118 W.-W. Tsai, I. D. Tevis, A. S. Tayi, H. Cui and S. I. Stupp, *J. Phys. Chem. B*, 2010, **114**, 14778–14786.
119 I. D. Tevis, W.-W. Tsai, L. C. Palmer, T. Aytun and S. I. Stupp, *ACS Nano*, 2012, **6**, 2032–2040.
120 A. Ruiz-Carretero, T. Aytun, C. J. Bruns, C. J. Newcomb, W.-W. Tsai and S. I. Stupp, *J. Mater. Chem. A*, 2013, **1**, 11674–11681.
121 T. Aytun, L. Barreda, A. Ruiz-Carretero, J. A. Lehrman and S. I. Stupp, *Chem. Mater.*, 2015, **27**, 1201–1209.
122 A. Ruiz-Carretero, Y. Atoini, T. Han, A. Operamolla, S. Ippolito, C. Valentini, S. Carrara, S. Sinn, E. A. Prasetyanto, T. Heiser, P. Samorì, G. Farinola and L. De Cola, *J. Mater. Chem. A*, 2019, **7**, 16777–16784.
123 S. Mula, T. Han, T. Heiser, P. Lévêque, N. Leclerc, A. P. Srivastava, A. Ruiz-Carretero and G. Ulrich, *Chem. – Eur. J.*, 2019, **25**, 8304–8312.
124 N. R. Ávila-Rovelo, G. Martinez, W. Matsuda, S. Sinn, P. Lévêque, D. Schwaller, P. Mésini, S. Seki and A. Ruiz-Carretero, *J. Phys. Chem. C*, 2022, **126**, 10932–10939.
125 G. Martinez, I. Id-boubrik, W. Matsuda, C. C. Carmona-Vargas, K.-I. Hong, C. Munuera, S. Seki and A. Ruiz-Carretero, *Chem. – Eur. J.*, 2024, **30**, e202400392.
126 J. Yao, C. Yu, Z. Liu, H. Luo, Y. Yang, G. Zhang and D. Zhang, *J. Am. Chem. Soc.*, 2016, **138**, 173–185.
127 R. Marty, R. Nigon, D. Leite and H. Frauenrath, *J. Am. Chem. Soc.*, 2014, **136**, 3919–3927.
128 J. López-Andarias, M. J. Rodriguez, C. Atienza, J. L. López, T. Mikie, S. Casado, S. Seki, J. L. Carrascosa and N. Martín, *J. Am. Chem. Soc.*, 2015, **137**, 893–897.
129 F. Li, K. G. Yager, N. M. Dawson, J. Yang, K. J. Malloy and Y. Qin, *Macromolecules*, 2013, **46**, 9021–9031.
130 F. Li, K. G. Yager, N. M. Dawson, Y.-B. Jiang, K. J. Malloy and Y. Qin, *Polym. Chem.*, 2015, **6**, 721–731.
131 F. Li, N. M. Dawson, Y.-B. Jiang, K. J. Malloy and Y. Qin, *Polymer*, 2015, **76**, 220–229.
132 T. L. Nguyen, S. Song, S.-J. Ko, H. Choi, J.-E. Jeong, T. Kim, S. Hwang, J. Y. Kim and H. Y. Woo, *J. Polym. Sci., Part A: Polym. Chem.*, 2015, **53**, 854–862.
133 M. González-Sánchez, M. J. Mayoral, V. Vázquez-González, M. Paloncýová, I. Sancho-Casado, F. Aparicio, A. de Juan, G. Longhi, P. Norman, M. Linares and D. González-Rodríguez, *J. Am. Chem. Soc.*, 2023, **145**, 17805–17818.
134 M. M. Safont-Sempere, G. Fernández and F. Würthner, *Chem. Rev.*, 2011, **111**, 5784–5814.
135 P. N. Taylor and H. L. Anderson, *J. Am. Chem. Soc.*, 1999, **121**, 11538–11545.
136 L. Schmidt-Mende, A. Fechtenkötter, K. Müllen, E. Moons, R. H. Friend and J. D. MacKenzie, *Science*, 2001, **293**, 1119–1122.
137 S. Prasanthkumar, S. Ghosh, V. C. Nair, A. Saeki, S. Seki and A. Ajayaghosh, *Angew. Chem. Int. Ed.*, 2015, **54**, 946–950.
138 J.-W. Lee, S. Seo, S.-W. Lee, G.-U. Kim, S. Han, T. N.-L. Phan, S. Lee, S. Li, T.-S. Kim, J.-Y. Lee and B. J. Kim, *Adv. Mater.*, 2022, **34**, 2207544.
139 F. Zhang, V. Lemaur, W. Choi, P. Kafle, S. Seki, J. Cornil, D. Beljonne and Y. Diao, *Nat. Commun.*, 2019, **10**, 4217.
140 W. Wei, C. e Zhang, Z. Chen, W. Chen, G. Ran, G. Pan, W. Zhang, P. Müller-Buschbaum, Z. Bo, C. Yang and Z. Luo, *Angew. Chem. Int. Ed.*, 2024, **63**, e202315625.
141 M. Kim, W.-T. Park, S. A. Park, C. W. Park, S. U. Ryu, D. H. Lee, Y.-Y. Noh and T. Park, *Adv. Funct. Mater.*, 2019, **29**, 1805994.
142 Y. Gao, Y. Deng, H. Tian, J. Zhang, D. Yan, Y. Geng and F. J. A. M. Wang, *Adv. Mater.*, 2017, **29**, DOI: 10.1002/adma.201606823.
143 W. Zhang, K. Shi, J. Huang, D. Gao, Z. Mao, D. Li and G. Yu, *Macromolecules*, 2016, **49**, 2582–2591.
144 B. Kang, R. Kim, S. B. Lee, S.-K. Kwon, Y.-H. Kim and K. Cho, *J. Am. Chem. Soc.*, 2016, **138**, 3679–3686.
145 X. Wang, S. Liu, C. Ren, L. Cao, W. Zhang and T. Wu, *Macromolecules*, 2022, **55**, 6415–6425.
146 A. Stefani, T. Salzillo, P. R. Mussini, T. Benincori, M. Innocenti, L. Pasquali, A. C. Jones, S. Mishra and C. Fontanesi, *Adv. Funct. Mater.*, 2024, **34**, 2308948.
147 X. Niu, R. Zhao, S. Yan, Z. Pang, H. Li, X. Yang and K. Wang, *Small*, 2023, **19**, 2303059.
148 F. García, R. Gómez and L. Sánchez, *Chem. Soc. Rev.*, 2023, **52**, 7524–7548.
149 T. S. Metzger, H. Batchu, A. Kumar, D. A. Fedotov, N. Goren, D. K. Bhowmick, I. Shioukhi, S. Yochelis, I. Schapiro, R. Naaman, O. Gidron and Y. Paltiel, *J. Am. Chem. Soc.*, 2023, **145**, 3972–3977.
150 R. Naaman and D. H. Waldeck, *J. Phys. Chem. Lett.*, 2024, **15**, 11002–11006.
151 B. Shen, Y. Kim and M. Lee, *Adv. Mater.*, 2020, **32**, 1905669.
152 S. Das and A. Ajayaghosh, *Small*, 2025, **21**, e07210.
153 M. Kataria and S. Seki, *Chem. – Eur. J.*, 2025, **31**, e202403460.
154 Q. Cheng, A. Hao and P. Xing, *Nat. Commun.*, 2021, **12**, 6320.
155 M. Liu, L. Zhang and T. Wang, *Chem. Rev.*, 2015, **115**(15), 7304–7397.
156 W. Chen, K. Ma, P. Duan, G. Ouyang, X. Zhu, L. Zhang and M. Liu, *Nanoscale*, 2020, **12**, 19497–19515.
157 M. Stolte, S.-L. Suraru, P. Diemer, T. He, C. Burschka, U. Zschieschang, H. Klauk and F. Würthner, *Adv. Funct. Mater.*, 2016, **26**, 7415–7422.
158 T. He, P. Leowanawat, C. Burschka, V. Stepanenko, M. Stolte and F. Würthner, *Adv. Mater.*, 2018, **30**, 1804032.
159 M. Makala, Z. Xu, S. Saiev, X. Ni, S. Sabury, V. Coropceanu, J.-L. Brédas, Y. Diao, J. R. Reynolds, O. D. Jurchescu and A. M. Österholm, *Chem. Mater.*, 2025, **37**, 4145–4157.
160 L. Liu, Y. Yang, S. C. J. Meskers, Q. Wang, L. Zhang, C. Yang, J. Zhang, L. Zhu, Y. Zhang and Z. Wei, *Adv. Mater.*, 2023, **35**, 2304627.
161 L. Liu, Y. Yang, Y. Wang, M. A. Adil, Y. Zhao, J. Zhang, K. Chen, D. Deng, H. Zhang, K. Amin, Y. Wu, Y. Zhang and Z. Wei, *ACS Mater. Lett.*, 2022, **4**, 401–409.
162 P. A. Hume, J. P. Monks, F. Pop, E. S. Davies, R. C. I. MacKenzie and D. B. Amabilino, *Chem. – Eur. J.*, 2018, **24**, 14461–14469.
163 G. Pancotti, C. E. Killalea, T. W. Rees, L. Liirò-Peluso, S. Riera-Galindo, P. H. Beton, M. Campoy-Quiles, G. Siligardi and D. B. Amabilino, *Nanoscale*, 2025, **17**, 3133–3144.
164 D. H. Waldeck, R. Naaman and Y. Paltiel, *APL Mater.*, 2021, **9**(4), 040902.
165 R. Gupta, A. Balo, R. Garg, A. K. Mondal, K. B. Ghosh and P. Chandra Mondal, *Chem. Sci.*, 2024, **15**, 18751–18771.
166 R. Naaman, Y. Paltiel and D. H. Waldeck, *Nat. Rev. Chem.*, 2019, **3**, 250–260.
167 A. M. Garcia, G. Martínez and A. Ruiz-Carretero, *Front. Chem.*, 2021, **9**, 722727.
168 Z. Shang, T. Liu, Q. Yang, S. Cui, K. Xu, Y. Zhang, J. Deng, T. Zhai and X. Wang, *Small*, 2022, **18**, 2203015.
169 M. Volpi, R. Jouclas, J. Liu, G. Liu, L. Catalano, N. McIntosh, M. Bardini, C. Gatsios, F. Modesti, N. Turetta, D. Beljonne, J. Cornil, A. R. Kennedy, N. Koch, P. Erk, P. Samorì, G. Schweicher and Y. H. Geerts, *Adv. Sci.*, 2023, **10**, 2301914.

170 R. Sun, K. S. Park, A. H. Comstock, A. McConnell, Y.-C. Chen, P. Zhang, D. Beratan, W. You, A. Hoffmann, Z.-G. Yu, Y. Diao and D. Sun, *Nat. Mater.*, 2024, **23**, 782–789.
171 P. S. Fernando, Y.-C. Chen, J. M. Baek and Y. Diao, *Annu. Rev. Chem. Biomol. Eng.*, 2025, **16**, 59–91.
172 P. Metrangolo, F. Meyer, T. Pilati, G. Resnati and G. Terraneo, *Angew. Chem. Int. Ed.*, 2008, **47**, 6114–6127.
173 M.-P. Zhuo, Y.-C. Tao, X.-D. Wang, Y. Wu, S. Chen, L.-S. Liao and L. Jiang, *Angew. Chem. Int. Ed.*, 2018, **57**, 11300–11304.
174 R. Gutzler, C. Fu, A. Dadvand, Y. Hua, J. M. MacLeod, F. Rosei and D. F. J. N. Perepichka, *Nanoscale*, 2012, **4**, 5965–5971.
175 L. Bai, P. Bose, Q. Gao, Y. Li, R. Ganguly and Y. Zhao, *J. Am. Chem. Soc.*, 2017, **139**, 436–441.
176 S. N. Afraj, C.-C. Lin, A. Velusamy, C.-H. Cho, H.-Y. Liu, J. Chen, G.-H. Lee, J.-C. Fu, J.-S. Ni, S.-H. Tung, S. Yau, C.-L. Liu, M.-C. Chen and A. Facchetti, *Adv. Funct. Mater.*, 2022, **32**, 2200880.
177 K. Kawabata and K. Takimiya, *Chem. Mater.*, 2023, **35**, 7628–7642.
178 Y. I. Park, C.-Y. Kuo, J. S. Martinez, Y.-S. Park, O. Postupna, A. Zhugayevych, S. Kim, J. Park, S. Tretiak and H.-L. Wang, *ACS Appl. Mater. Interfaces*, 2013, **5**, 4685–4695.
179 M. Schwarze, K. S. Schellhammer, K. Ortstein, J. Benduhn, C. Gaul, A. Hinderhofer, L. Perdigón Toro, R. Scholz, J. Kublitski, S. Roland, M. Lau, C. Poelking, D. Andrienko, G. Cuniberti, F. Schreiber, D. Neher, K. Vandewal, F. Ortmann and K. Leo, *Nat. Commun.*, 2019, **10**, 2466.
180 L.-J. Chen and H.-B. Yang, *Acc. Chem. Res.*, 2018, **51**, 2699–2710.
181 X. Liu, E. K. Lee, D. Y. Kim, H. Yu and J. H. Oh, *ACS Appl. Mater. Interfaces*, 2016, **8**, 7291–7299.
182 H. Xu, J. Song, P. Zhou, Y. Song, J. Xu, H. Shen, S. Fang, Y. Gao, Z. Zuo, J. M. Pina, O. Voznyy, C. Yang, Y. Hu, J. Li, J. Du, E. H. Sargent and F. Fan, *Nat. Photonics*, 2024, **18**, 186–191.